LILRB4 represents a promising target for immunotherapy by dual targeting tumor cells and myeloid-derived suppressive cells in multiple myeloma

Lixin Gong,[1,2*] Hao Sun,[1,2*] Lanting Liu,[1,2] Xiyue Sun,[1,2] Teng Fang,[1,2] Zhen Yu,[1,2] Weiwei Sui,[1,2] Jingyu Xu,[1,2] Tingyu Wang,[1,2] Fangshuo Feng,[1,2] Lei Lei,[3] Wei Rui,[3] Yuxuan Liu,[1,2] Xueqiang Zhao,[4] Gang An,[1,2] Xin Lin,[4] Lugui Qiu[1,2] and Mu Hao[1,2]

[1]State Key Laboratory of Experimental Hematology, National Clinical Research Center for Blood Diseases, Haihe Laboratory of Cell Ecosystem, Institute of Hematology & Blood Diseases Hospital, Chinese Academy of Medical Sciences & Peking Union Medical College, Tianjin; [2]Tianjin Institutes of Health Science, Tianjin; [3]BriSTAR Immunotech Biotechnology Co. Ltd., Beijing and [4]Department of Basic Medical Sciences, Tsinghua University School of Medicine, Beijing, China

**LG and HS contributed equally as first authors.*

Correspondence: M. Hao
haomu@ihcams.ac.cn

L. Qiu
qiulg@ihcams.ac.cn

X. Lin
linxin307@tsinghua.edu.cn

Received: January 20, 2024.
Accepted: May 20, 2024.
Early view: May 30, 2024.

https://doi.org/10.3324/haematol.2024.285099

Abstract

Multiple myeloma (MM) remains an incurable hematologic malignancy. Despite tremendous advances in the treatment of this disease, about 10% of patients still have very poor outcomes with a median overall survival of less than 24 months. Our study aimed to underscore the critical mechanisms pertaining to rapid disease progression and provide novel therapeutic choices for these ultrahigh-risk patients. We utilized single-cell transcriptomic sequencing to dissect the characteristic bone marrow niche of patients who survived less than 2 years (EM24). Notably, enrichment of a LILRB4^{high} pre-mature plasma-cell cluster was observed in EM24 patients compared to patients with durable remission. This cluster exhibited aggressive proliferation and a drug-resistance phenotype. High levels of LILRB4 promoted MM clonogenicity and progression. Clinically, high expression of LILRB4 was correlated with poor prognosis in both newly diagnosed MM patients and relapsed/refractory MM patients. ATAC-sequencing analysis identified that pronounced chromosomal accessibility caused the elevation of LILRB4 on MM cells. CRISPR-Cas9 deletion of *LILRB4* alleviated the growth of MM cells, inhibited the immunosuppressive function of myeloid-derived suppressive cells (MDSC), and further rescued T-cell dysfunction in the MM microenvironment. Greater infiltration of MDSC was observed in EM24 patients. We therefore generated an innovative T-cell receptor-based chimeric antigen receptor T cell, LILRB4-STAR-T. Cytotoxicity experiments demonstrated that LILRB4-STAR-T cells efficaciously eliminated tumor cells and impeded MDSC function. In conclusion, our study elucidates that LILRB4 is an ideal biomarker and promising immunotherapy target for high-risk MM. LILRB4-STAR-T-cell immunotherapy is promising against both tumor cells and the immunosuppressive tumor microenvironment in MM.

Introduction

Advances in the treatment of multiple myeloma (MM) have greatly improved the outcome of affected patients in the past decades, but MM is still an incurable disease. Although several studies have shown that the median overall survival (OS) has reached over 10 years for newly diagnosed MM (NDMM) patients treated with bortezomib, lenalidomide and dexamethasone, about 20% to 30% of the patients survive less than 3 years.[1-3] These patients are defined as having high-risk MM and include those who die within 24 months; this group of patients with early mortality (EM24) are regarded as having ultrahigh-risk MM.[4-6] How to identify and treat ultrahigh-risk patients is a major challenge in clinical practice. The main approaches to circumvent the bottleneck of identifying and treating these MM patients include: (i) clarifying the specific biological characteristics of ultrahigh-risk patients with an OS of less than 2 years, thereby uncovering mechanisms of refractory MM and drug resistance; (ii) identifying specific biomarkers as well as

novel therapeutic targets for ultrahigh-risk patients; and (iii) developing new effective drugs by conducting more in-depth biological research, implementing individualized treatment strategies for these patients, including prioritizing chimeric antigen receptor (CAR) T-cell therapy and bispecific antibody immunotherapy, etc.

Genome instability and an immunosuppressive tumor microenvironment (TME) are important features of the development and progression of MM.[7-9] During the disease process, sequential genetic hits can be induced by disease progression and treatment pressure, and further increase the intra-tumoral heterogeneity of the MM cells.[10] Notably, microenvironmental changes can provide a premalignant niche that precedes the acquisition of any genetic aberration.[11-14] The TME in MM is characterized by a selective reduction in cytotoxic memory T cells and an increase in several immunosuppressive cell populations, such as regulatory T cells and myeloid-derived suppressive cells (MDSC).[15] The crosstalk between tumor cells and the microenvironment further supports tumor growth and influences tumor evolution.[16,17] Therefore, targeting both MM cells and the tumor-promoting microenvironment would be the ideal strategy to cure myeloma.

In this study, we investigated, at single-cell resolution, the heterogeneity of bone marrow mononuclear cells (BMMC) from 12 NDMM patients with diverse clinical features. A precursor plasma-cell cluster with high expression of leukocyte immunoglobulin-like receptor subfamily B member 4 (LILRB4) was enriched in EM24 patients and correlated strongly with diseaseaggressiveness, drug resistance, and poor outcomes of both NDMM and relapsed/refractory MM (RRMM) patients. *In vitro* and *in vivo* studies demonstrated that LILRB4 plays a critical role in MM pathogenesis. Additionally, LILRB4^{high} MM cells induce the generation of MDSC. Importantly, we generated an innovative T-cell receptor (TCR)-based CAR-T cell, named STAR (synthetic TCR and antigen receptor)-T cell, to target LILRB4^{+} MM cells and LILRB4^{+} MDSC. LILRB4-STAR-T cells exhibited ideal cytotoxicity against MM by targeting MM cells and MDSC in the immunosuppressive TME. Altogether, our study demonstrated that *LILRB4* is an ultrahigh-risk gene and a promising target of immunotherapy in MM via dual targeting of myeloma cells and MDSC in the TME.

Methods

The complete methods are provided in the *Online Supplementary File*.

Patients' characteristics and single-cell RNA-sequencing strategy

BMMC were obtained from seven healthy donors and 12 patients with NDMM. The clinical and biological characteristics of the 12 MM patients are listed in *Online Supplementary Figure S1A*. This study was conducted according to the guidelines of the Declaration of Helsinki and approved by the ethics review board of the Institute of Hematology and Blood Diseases Hospital, Chinese Academy of Medical Sciences (China) (protocol code KT2020010-EC-2). Written informed consent was obtained from all subjects involved in the study before sample collection.

Single-cell RNA sequencing and data analysis

The full process and methods for sample collection and single-cell preparation, single-cell RNA library preparation and sequencing, and processing of the single-cell (sc) RNA-sequencing data are provided in the *Online Supplementary Methods*. Dimensionality reduction, clustering of cells, and visualization were performed as in our previous study.[14,18] Cell clusters were annotated using the expression of specific marker genes.

H3K27ac and H3K27me3 chromatin immunoprecipitation sequencing

Chromatin immunoprecipitation (ChIP) sequencing reads of H3K27ac and H3K27me3 from PRJNA608681[19] and PRJNA231147[20] were aligned to the hg19 genome using BWA (v 0.7.12). Uniquely mapped peaks and their signal intensity were obtained using MACS version 2.1.0 with default parameters. Input BAM files were used as controls, and peaks with a q-value threshold of 0.05 were considered significant. ChIPseeker[21] was utilized to identify the nearest genes around the peaks based on the transcriptional start site. Genes were considered enriched for H3K27ac or H3K27me3 if a peak was detected up to 3 kb up- or down-stream of the transcriptional start site.

Manufacturing of STAR-T cells

LILRB4 STAR was generated based on homemade LILRB4-specific nanobodies. The STAR-T-cell structure is presented in *Online Supplementary Figure S7A*. Lenti-X-293T cells for lentivirus packaging were purchased from Takara Biomedical Technology Company. Lentivirus vectors (pHAGE) were used in the study. T cells were isolated using an EasySep negative selection kit (Stemcell Technologies) from peripheral blood mononuclear cells from healthy donors. T cells were first stimulated with precoated anti-CD3, anti-CD28, and human fibronectin. After being activated for 24 h, the cells were transduced with concentrated virus. The transduction efficiency was determined 4 days later. T cells were cultured at a concentration of 1-3×10^{6} cells/mL, with half of the culture medium replaced every other day during T-cell expansion.[22]

In vivo study

The *in vivo* study was performed according to our previous study. Briefly, 1×10^{7} H929 wild-type cells were injected subcutaneously. Mice were treated with 1×10^{7} LILRB4-STAR-T cells or mock-T cells when the average tumor size reached

100 mm^3. Tumor size was measured every other day and calculated with the formula: 0.52 × length × $width^2$ (mm^3). *in vivo* studies were performed in accordance with protocols approved by the Institutional Animal Care and Use Committee of the Institute of Hematology, Chinese Academy of Medical Sciences (Tianjin, China).

Statistical analysis

Data were analyzed using R language and GraphPad Prism 8.0 software. Statistical significance was set at $P<0.05$.

Results

Single-cell transcriptomic profiling of the bone marrow ecosystem in multiple myeloma patients with different clinical features

We included 12 MM patients with different clinical features in this study. A single-cell transcriptomic overview of BMMC from 12 NDMM patients was compared with that of seven healthy donors (Figure 1A). The clinical and pathological details of the MM patients are summarized in *Online Supplementary Figure S1A*. Among these 12 patients, four had rapid disease progression and a short survival of less than 24 months; these patients with early mortality were classified as clinically ultrahigh-risk and defined as the EM24 group. The other eight patients formed the non-EM24 (nEM24) group. Principal component dimensionality reduction analysis demonstrated the significant difference in cell clustering between healthy donors, the EM24 group, and the nEM24 group (Figure 1B). All patients were risk stratified by the International Staging System (ISS) and its revision (R-ISS) and received combination therapy with bortezomib, lenalidomide and dexamethasone. All four patients in the EM24 group had ISS stage III disease and harbored 1q+, a high-risk cytogenetic abnormality.[23] Two of the four EM24 patients were classified as having R-ISS stage III disease and had two of the following cytogenetic abnormalities, 1q+, del (17p) and t(4;14), which define double-hit myeloma.[24] However, in the nEM24 group, five of eight patients were in ISS stage III and three patients had R-ISS stage III double-hit myeloma, with the simultaneous presence of 1q+ and t(4;14). Given the clinical diversity of these patients, factors other than cytogenetic abnormalities affect myeloma aggressiveness and clinical outcomes.

In a scRNA-sequencing study, 42,936 cells were analyzed; an average of 7,939 unique molecular identifiers and 1,243 genes were generated per single cell (*Online Supplementary Figure S1B*). After correction for a batch effect, a total of 16 diverse major bone marrow cell types (clusters 0-15) were identified (Figure 1C), including hematopoietic stem cells (HSC, cluster 10/*CD34*), early erythroid cells (clusters 5 and 6/*GATA1*), late erythroid cells (clusters 1, 8, and 12/*HBA1*), myeloid cells (clusters 4, 9, and 15/CD14, *LYZ*), NK cells (cluster 2/*NKG7*), T cells (cluster 3/*CD3D*), B-cell progenitors (cluster 11/*MME*), B cells (cluster 7/*CD19*, *MS4A1*), and plasma/MM cells (clusters 0, 4, and 13/*SDC1*, *TNFRSF17*) (*Online Supplementary Figure S1C*). The correlation of gene expression among the 16 cell clusters is shown in *Online Supplementary Figure S1D*.

The proportion of myeloma/plasma cells was obviously greater in MM patients than in healthy donors. Notably, according to the odds ratio (OR) analysis, myeloma/plasma cells showed a stronger distribution preference in EM24 patients compared to nEM24 patients. Interestingly, B cells were less distributed in EM24 patients than in nEM24 patients ($P<0.05$), indicating potential aberrant B-cell development and differentiation in EM24 patients. In addition, erythroid cells appeared to decrease in MM patients compared with healthy donors, consistent with our previous study revealing that malignant plasma cells could impede erythropoiesis and result in anemia in MM.[25] Of note, a smaller proportion of myeloid cells was found in MM patients. However, myeloid cells appeared to be more enriched in EM24 patients than in nEM24 patients (Figure 1D, E). Taken together, EM24 patients had enrichment of MM/plasma cells and myeloid cells, whereas they had a lower infiltration of T/NK cells and erythroid cells.

Enrichment of sub-C4 plasma cells in EM24 multiple myeloma patients

We next sought to identify intrinsic differences between MM cells from patients in the EM24 and nEM24 groups. We integrated the MM/plasma cell compartment from all samples into a joint dataset. A total of ten heterogeneous subclusters (sub-C0-9) were identified (Figure 2A). According to light chain restriction analysis, all the clusters were light chain-restricted, except for sub-C7, and also highly expressed plasma cell marker genes, including *CD38*, *SDC1*, and *TNFRSF17* (Figure 2B, *Online Supplementary Figure S2A*, B). Samples from healthy donors only harbored sub-C7, which displayed a balanced light chain ratio. Thus, we inferred that sub-C7 was the normal plasma cell cluster, and the others were the malignant plasma cells. Notably, a significant increase of sub-C4 was present in EM24 patients compared with nEM24 patients (Figure 2C). The odds ratio analysis confirmed that sub-C4 displayed a specifically strong distribution preference in EM24 patients (Figure 2D). Importantly, we found that sub-C4 showed relatively higher levels of *CD19*, *CD27* and *CD24* genes, the marker genes of initiating tumor cells in MM compared with other plasma cell subclusters, indicating a phenotypically pre-mature state of sub-C4 (Figure 2B, *Online Supplementary Figure S2B*).[26] This finding suggested that EM24 patients had an enrichment of pre-mature plasma cells (sub-C4), which might be associated with the aggressive progression of disease in EM24 patients.

Aiming to further probe the characteristics of tumor cells pertaining to the shortened survival of EM24 patients, we analyzed differences in gene expression between MM cells

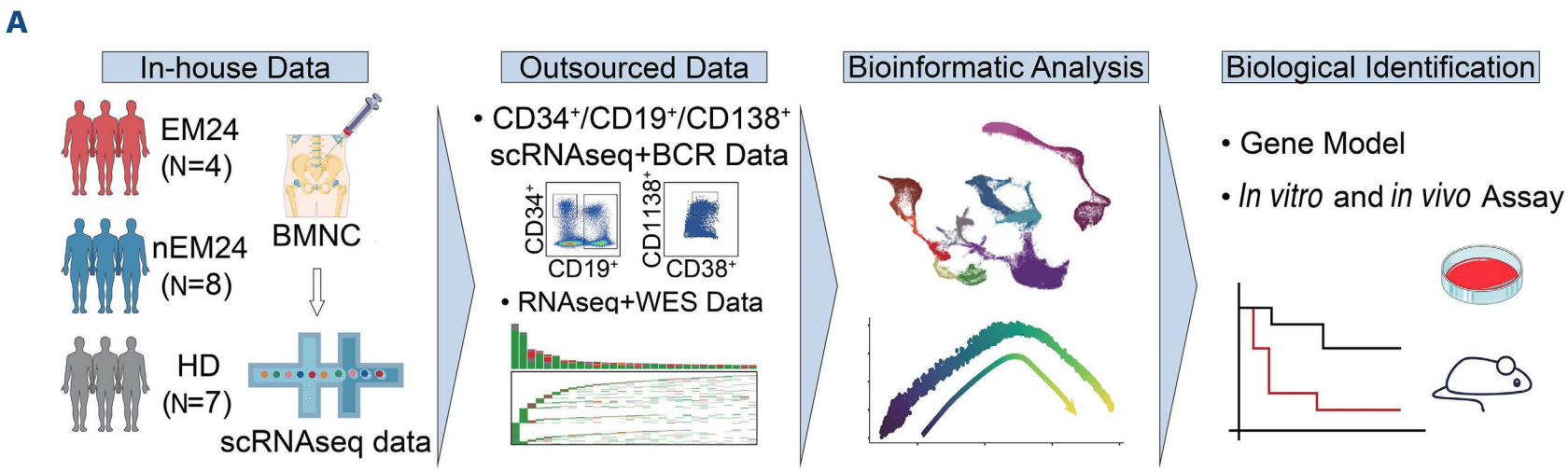

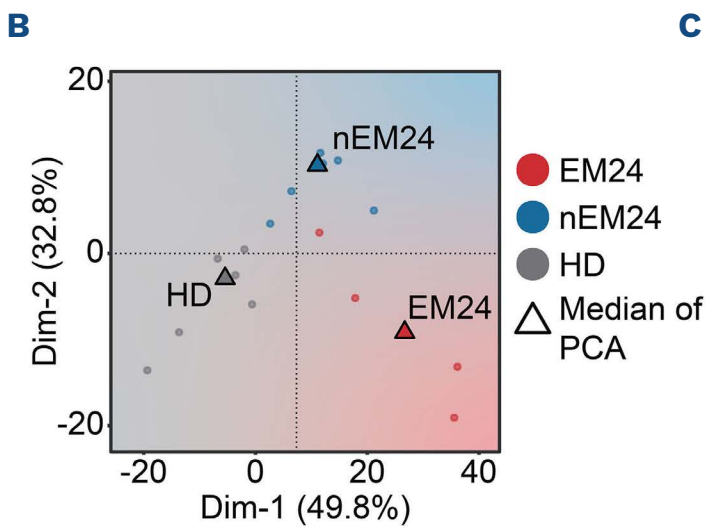

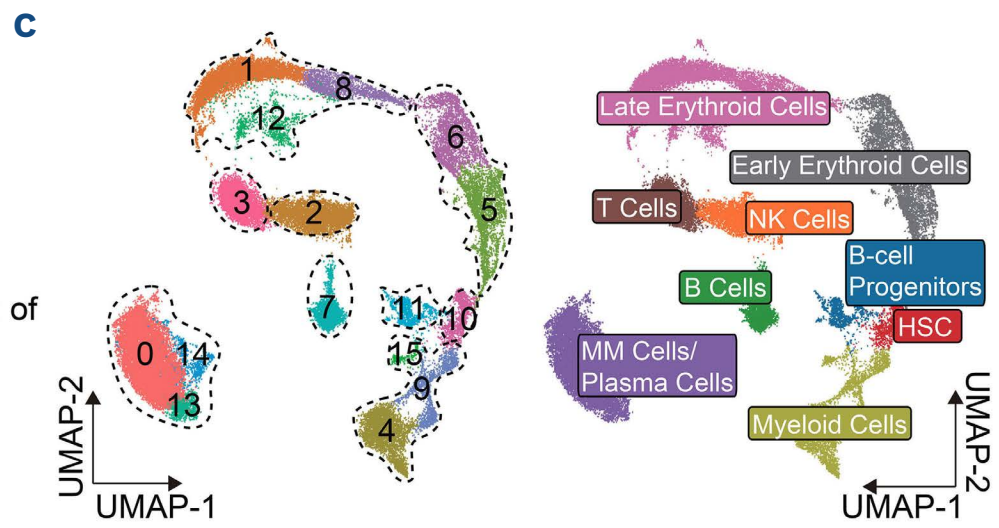

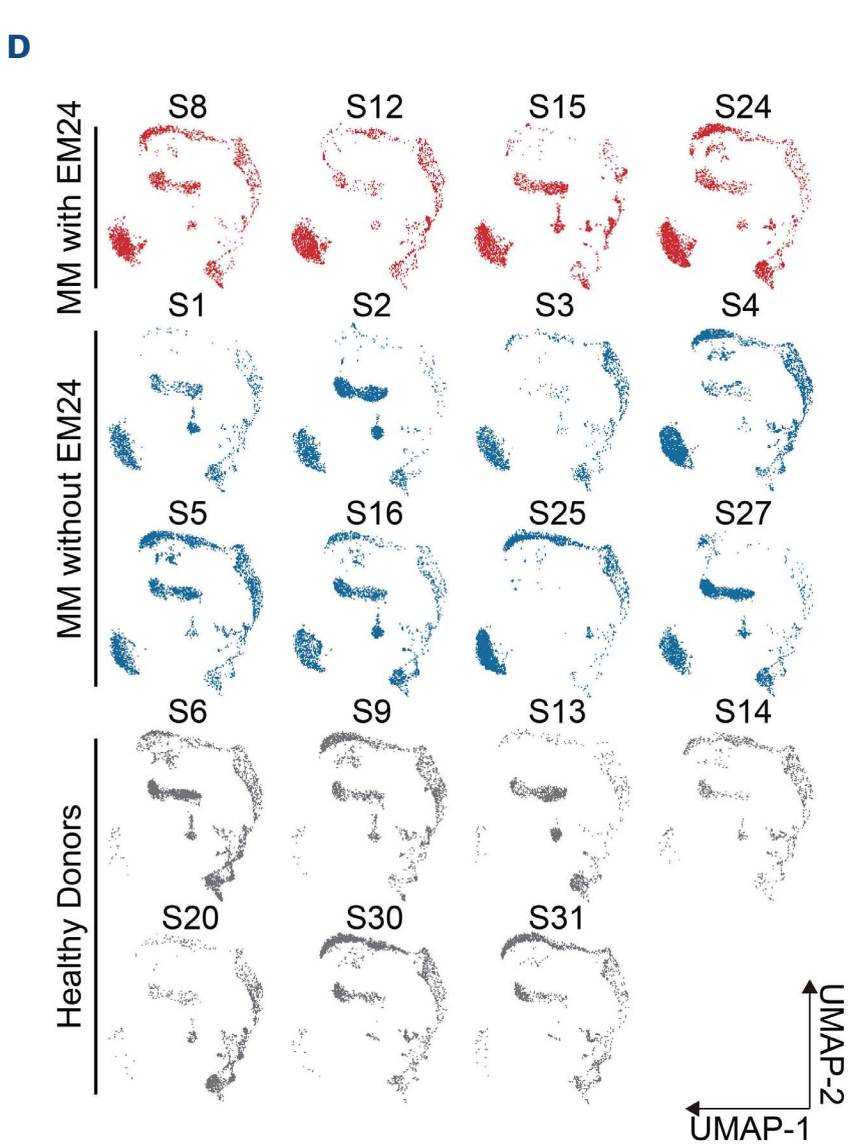

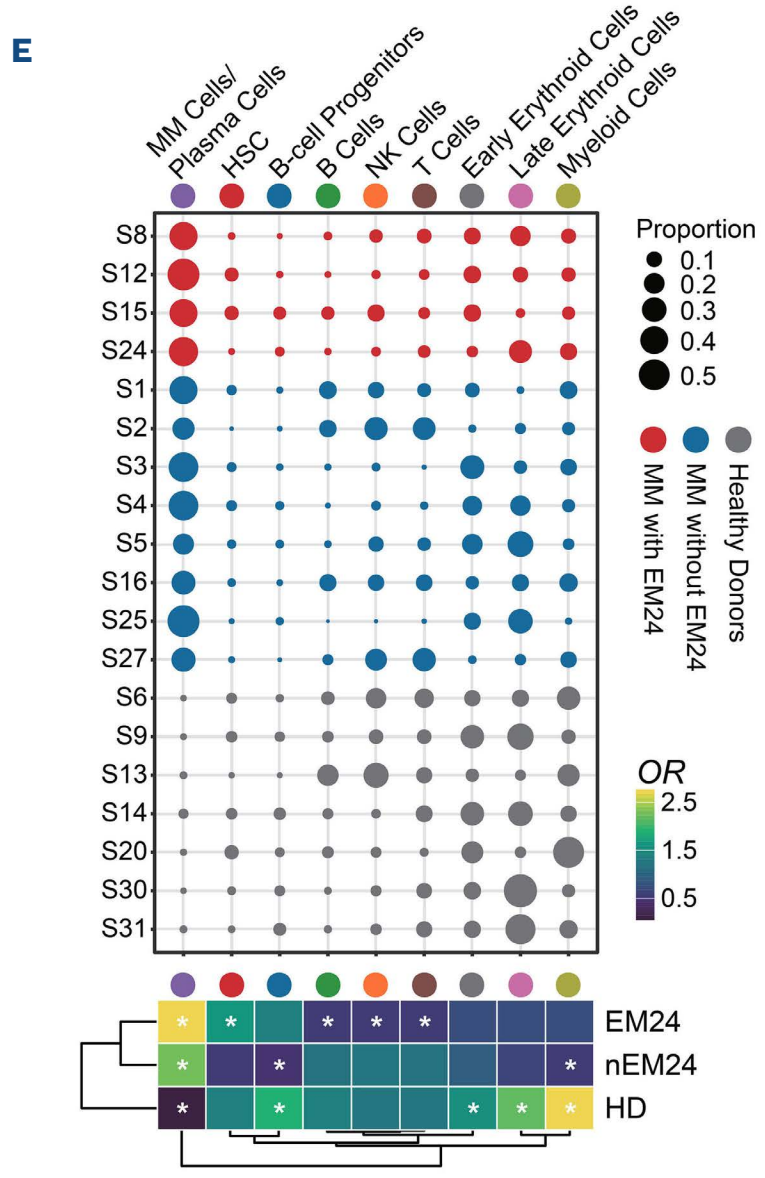

Continued on following page.

Figure 1. Single-cell transcriptomics profiling of the bone marrow ecosystem in patients with multiple myeloma. (A) Schematic representation of the experimental strategy based on in-house and outsourced data. Bone marrow mononuclear cells from seven healthy donors (HD), four patients with multiple myeloma who died within 24 months (EM24), and eight who did not die within 24 months (nEM24) were measured by 10× Genomics-based single-cell RNA sequencing. Multi-omics data and biological assays were applied to validate our findings. (B) Two-dimensional plots showing the distribution of each sample. The small circles represent individual patients, the color indicates the patients' group. Triangles represent the median of the principal component analysis. (C) Uniform manifold approximation and projection (UMAP) plots showing cell clusters (left panel) and cell annotation (right panel) by color. (D) UMAP projections of cells from each sample. Sample names and sample groups are labeled in the figure. (E) Top. Bubble plots showing the proportion of each cell type in each sample. Samples were divided into EM24 MM patients (red), nEM24 MM patients (blue), and HD (gray). Bottom. Heatmap plot illustrating the odds ratio (OR) for each cell in each sample group based on a Fisher exact test. A high OR with an asterisk indicates that the cell is more likely to distribute in the group, while a low OR with an asterisk indicates that the cell is less likely to distribute in the group. scRNAseq: single-cell RNA sequencing; BMNC: bone marrow mononuclear cells; BCR: B-cell receptor; WES: whole-exome sequencing; Dim: dimension; PCA: principal component analysis; MM: multiple myeloma; NK: natural killer; HSC: hematopoietic stem cells.

from EM24 and nEM24 patients, looking at a total of 20,711 genes from 12,835 cells. The upregulated genes in EM24 MM patients were mainly featured by sub-C4 cells (*Online Supplementary Figure S2C*).

We also conducted an analysis of the H3K27ac ChIP-sequencing data from CD138$^+$ MM cells derived from NDMM patients using the GSE145891 dataset. We identified genes with significant H3K27ac enrichment. Subsequently, we analyzed differentially expressed genes between the sub-C4 cluster and other MM-cell clusters. A total of 1,726 genes were observed to be upregulated in the sub-C4 cluster. Among these upregulated genes, 1,620 (93.86%) displayed significant H3K27ac enrichment. The top genes regulated by H3K27ac are listed in *Online Supplementary Table S1*. Interestingly, the upregulated genes of sub-C4 were mainly regulated by H3K27ac, while the downregulated genes of sub-C4 were regulated by H3K27me3 (Figure 2E).

We further inferred the differentiation stage of sub-C4 from the B-cell to plasma-cell differentiation paradigm. We downloaded the publicly available scRNA-sequencing data of normal B-cell differentiation and B-cell receptor (BCR) information which were utilized to construct a classifier for defining B-cell differentiation stages, but not compatible for plasma cells.[27-29] Next, we integrated scRNA-sequencing data and scBCR-sequencing data of HSC, B-cell lineage cells and plasma cells from healthy donors, and sequentially defined cell clusters along HSC to plasma-cell differentiation (*Online Supplementary Figure S2D-F*). A random-forest training approach was applied to construct a classifier that showed excellent ability to define the cell clusters of different stages from HSC to plasma cells (all area under the curve values >0.95) (*Online Supplementary Figure S2G*). We further generated the normal differentiation trajectory from HSC to plasma cells following pseudo-time analysis, enabling us to map our in-house scRNA-sequencing data of MM cells and identify the differentiation stages (*Online Supplementary Figure S3A, B*). Notably, our results showed that sub-C4 was enriched between the plasmablast stage and the terminal MM cell-cluster stage (Figure 2F, *Online Supplementary Figure S3C, D, F*). Additionally, gene set enrichment analysis of the upregulated genes in sub-C4 showed that the signaling pathways associated with stem cell differentiation and stemness (Wnt, Notch, and Hedgehog) were significantly enriched in sub-C4 (*Online Supplementary Figure S3E*). These findings strongly supported that a pre-mature differentiation stage of sub-C4 MM cells was enriched in the EM24 group of MM patients.

Genomic alterations and high-risk gene identification in sub-C4 plasma cells

Given the high proportion of pre-mature sub-C4 cells in the bone marrow of EM24 patients, we were interested in determining the genomic features of sub-C4 plasma cells in the pathogenesis of MM. We first utilized publicly available proliferation and drug-resistance associated gene sets to assess the different MM subclusters.[30-33] We found that the sub-C4 plasma-cell subcluster had the highest proliferation and drug-resistance scores from among ten heterogeneous MM-cell subclusters (Figure 3A). Copy number variation analysis showed that sub-C4 plasma cells exhibited the most complex cytogenetic abnormalities, including del(1p), del(2q), amp(5q), del(10q), amp(12p), del(13), del(14), del(17p), and amp(19) (Figure 3B). Furthermore, copy number variation score was higher in EM24 patients than in nEM24 ones (*Online Supplementary Figure S4A, B*). Additionally, we found that sub-C4 plasma cells had the highest mutation score among all the MM subclusters. *KRAS*, *NRAS*, and *FAM46C*/*TENT5C* were the top mutated genes in sub-C4 plasma cells. The most common type of mutation was missense mutations (Figure 3C). Consistently, further analysis showed that EM24 patients had higher mutation scores than nEM24 patients (*Online Supplementary Figure S4C, D*). The most enriched signaling pathways of sub-C4 included regulation of protein ubiquitination, immune effector processes, B-cell differentiation, and cell cycle process (Figure 3D). We further constructed a network analysis of transcription factors and downstream target genes using differentially expressed genes of sub-C4 plasma cells. We found that *MYC* and *E2F1* were highly activated transcription factors in sub-C4. *MYC* and *E2F1* were the critical transcription factors in regulating numerous downstream genes and played a critical role in promoting tumor growth. Gene co-expression

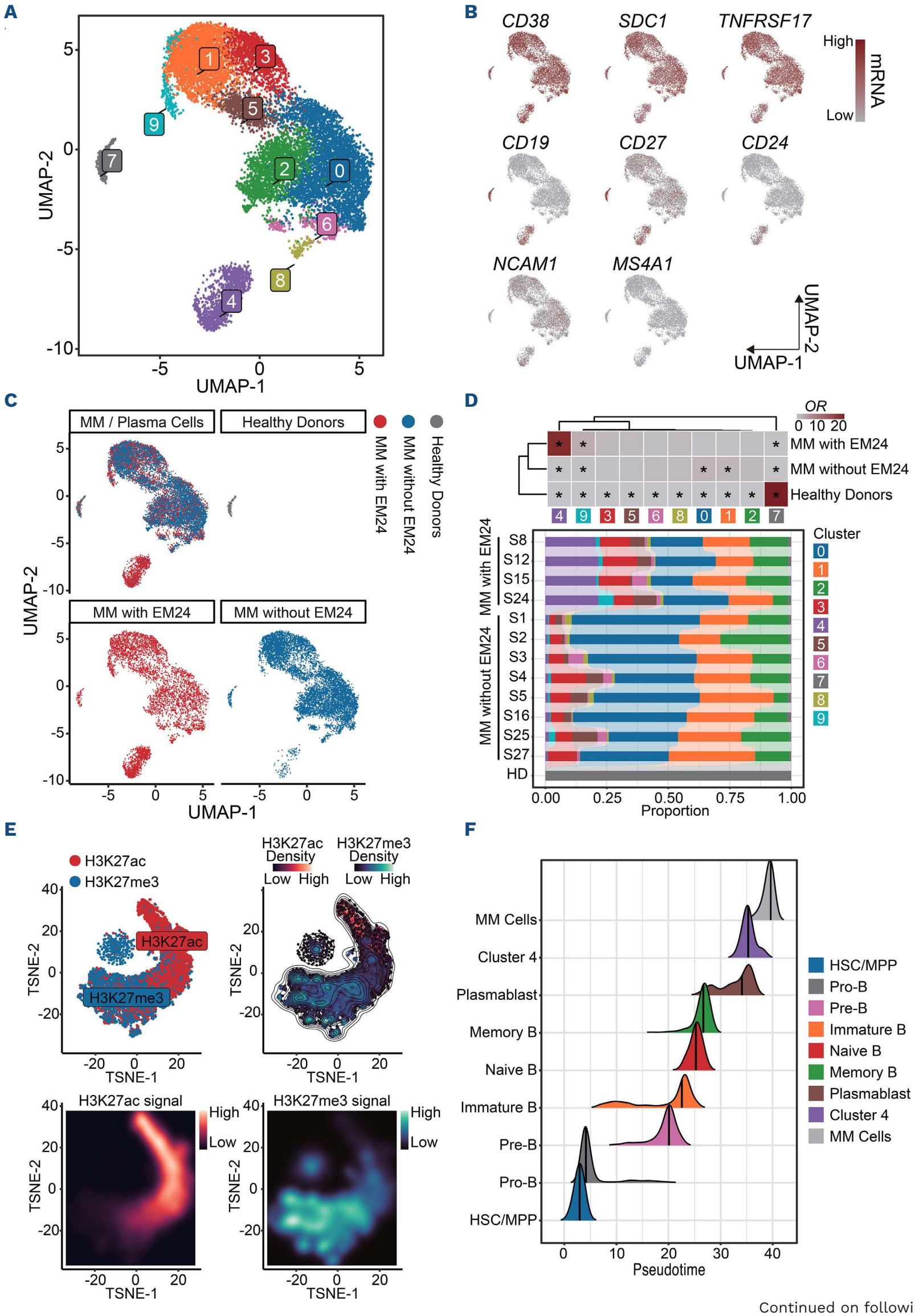

Continued on following page.

Figure 2. Characteristics of plasma cells in EM24 multiple myeloma patients. (A) Uniform manifold approximation and projection (UMAP) plot showing ten plasma cell clusters from all samples. (B) UMAP plots showing the expression of marker genes in plasma cells. (C) UMAP plots showing data for plasma cells from healthy donors, from multiple myeloma (MM) patients who died within 24 months (EM24), and from MM patients who did not die within 24 months (nEM24). (D) Top. Heatmap plot illustrating the odds ratio of each cluster in each sample group based on a Fisher exact test. Bottom. Bar plot showing the proportion of each cluster in each MM sample and healthy donor. (E) Top. T-distributed stochastic neighbor embedding point and density plots showing the distribution of epigenetically controlled genes. Bottom. Fitted density plot illustrating the H3K27ac-regulated and H3K27me3-regulated gene signal from chromatin immunoprecipitation sequencing data. (F) Density line plot showing the distribution of cells of plasma-cell lineage along with the pseudotime. HD: healthy donor; OR: odds ratio; TSNE: T-distributed stochastic neighbor embedded; HSC: hematopoietic stem cells cells; MPP: multipotent blood progenitors.

analysis further revealed four gene modules, ubiquitin, and proteosome, immune-regulation, B-cell differentiation, and cell cycle, including hub genes related to sub-C4, such as *LILRB4*, *CD74*, *XBP1*, *MKI67*, *AURKB*, and *USP1* (*Online Supplementary Figure S4E*). There are previous reports of a 70 high-risk gene set (UAMS-70) and a 92 high-risk gene set (SKY-92) in MM.[30,34] Interestingly, these two gene sets were most abundantly expressed in sub-C4, indicating that, from among the heterogenous subclusters of MM cells, sub-C4 plasma cells had the most aggressive potential for pro-

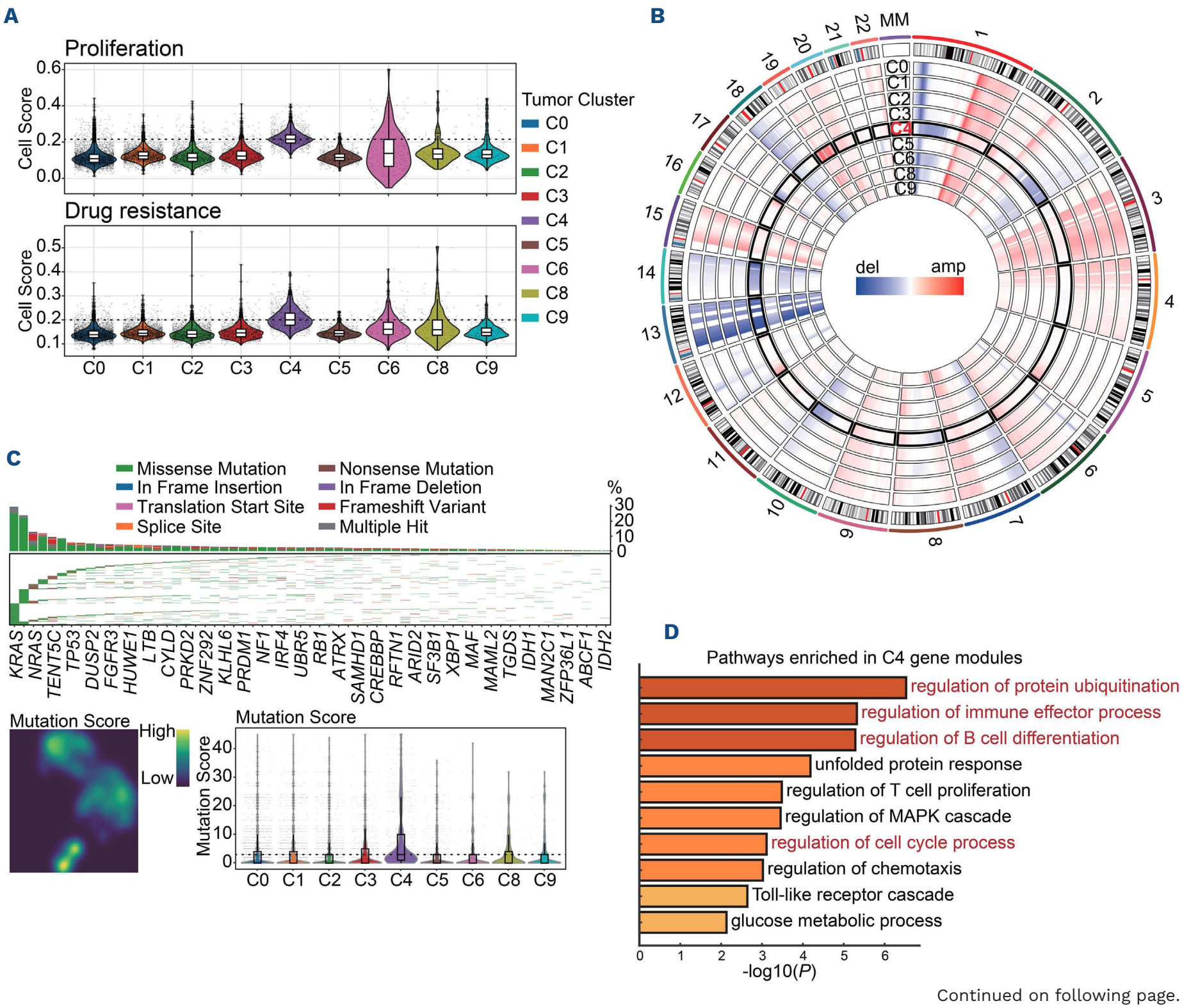

Continued on following page.

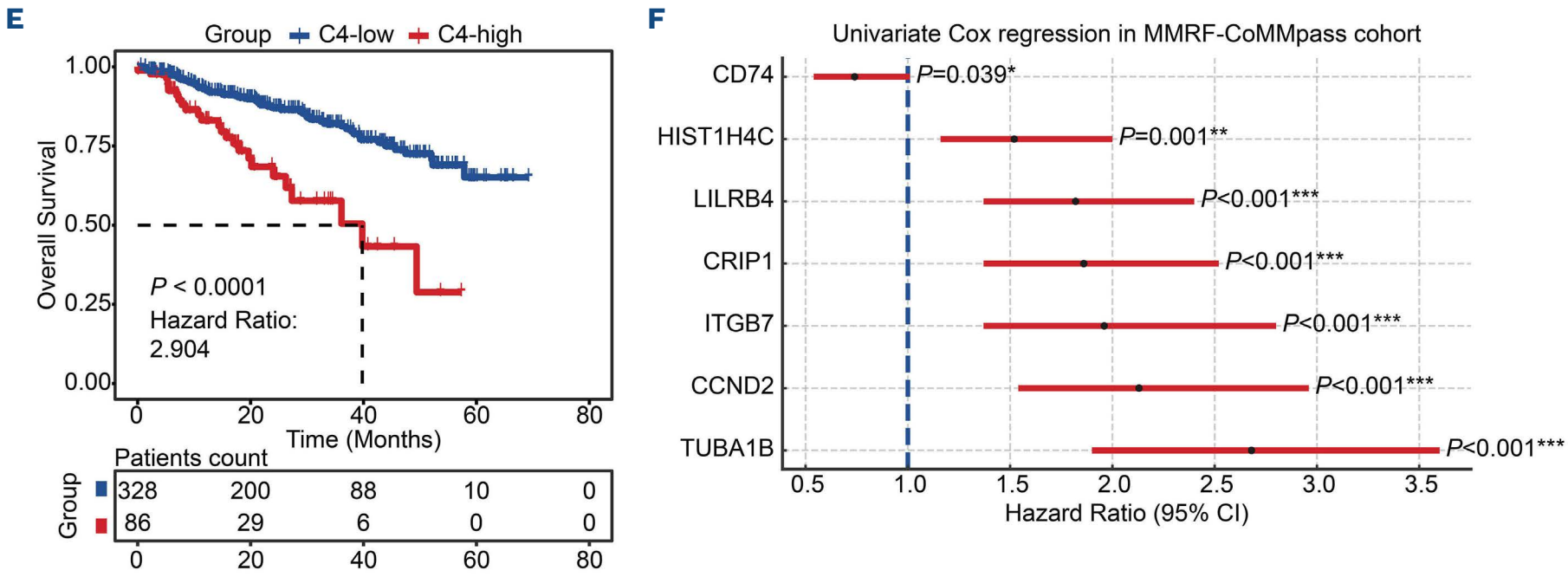

Figure 3. Genomic alterations and high-risk gene identification in sub-C4 plasma cells. (A) Violin plots showing the cell scores for proliferation and drug resistance in multiple myeloma (MM) cell clusters. (B) Circular genomic map illustrating copy number variations in MM cell clusters. Each lane indicates one cell cluster and the outmost lane indicates chromosome structure. Red represents amplification and blue represents deletion. (C) Top. Waterfall plot displaying 63 mutational driver genes in 947 MM patients of the MMRF-CoMMpass cohort. Bottom left. Fitted density plot showing mutational scores of driver genes in plasma cells. Bottom right. Violin plot showing the mutational score in MM cell clusters. (D) Bar chart showing enriched pathways in gene modules specific to sub-C4. The analysis was performed by Metascape. (E) Kaplan-Meier curves showing the overall survival of 414 MM patients with a high or low proportion of sub-C4 in the GSE2658. A log-rank test was applied for the comparison between groups. (F) Forest plot showing the hazard ratios (blue dots) and 95% confidence intervals (red lines), as determined by univariate Cox regression, for seven genes in the MMRF-CoMMpass cohort. *P<0.05, **P<0.01, ***P<0.001.

gression (*Online Supplementary Figure S4F*).

To confirm this hypothesis, the constitution of ten sub-clusters of MM/plasma cells derived from the scRNA-sequencing data analysis was imputed in each patient of the GSE2658 dataset (N=414) and MMRF-CoMMpass dataset (N=754). Survival analysis and Kaplan-Meier curves showed that patients with a high proportion of sub-C4 plasma cells had inferior outcomes (P<0.0001) (Figure 3E, *Online Supplementary Figure S4G*). These data support the concept that the proportion of sub-C4 plasma cells is a valuable predictive biomarker of inferior outcome in NDMM patients. Furthermore, these findings also suggest that the genomic alterations in sub-C4 contribute to the aggressive progression of disease and poor outcome of MM patients. L1 regularization analysis was next applied to investigate specific genomic alterations within sub-C4, which were identified from the transcription factor-gene network and gene co-expression network.[35] We found that seven genes were incorporated among the optimal features for discriminating the prognosis of MM patients (*Online Supplementary Figure S4H*). The genes were the top seven genes with high expression levels in sub-C4 plasma cells, including *LILRB4*, *TUBA1B*, *ITGB7*, *CRIP1, CCND2*, *HIST1H4C*, and *CD74*, which correlated strongly with poor outcome of MM patients. Hazard ratios were calculated, using both univariate and multivariate Cox proportional hazard models, in the MMRF-CoMMpass cohort. The hazard ratios for five genes (*LILRB4*, *TUBA1B*, *ITGB7*, *CRIP1*, and *CCND2*) were higher than 1.0. (Figure 3F, *Online Supplementary Figure S4I*). These data imply that the abundance of sub-C4 plasma cells in MM patients has prognostic value.

LILRB4 is a biomarker of aggressive multiple myeloma

Among the seven genes identified above, we noted that *LILRB4* was the most specifically highly expressed gene within sub-C4 (Figure 4A). To emphasize the association between *LILRB4* and the aggressive sub-C4 MM cluster, we classified plasma cells into sub-C4 and non-sub-C4 according to their expression of *LILRB4*, and generated a receiver operating characteristic curve. The area under curve value of sub-C4 by *LILRB4* was 0.85. At the optimal cutoff point, the sensitivity of *LILRB4* expression in distinguishing clusters reached 0.73, and the specificity reached 0.96 (*Online Supplementary Figure S5A*). Moreover, we found that the expression of *LILRB4* was high in the proliferation (PR) and MAF-high-level (MF) groups of MM patients (Figure 4B), which were high-risk groups in the UAMS-7 groups identified by Zhan *et al.*[36] When considering the correlation between *LILRB4* expression and disease progression, we found that *LILRB4* expression increased significantly with progression from the precursor stage to symptomatic MM according to the datasets in the Gene Expression Omnibus (GSE2658, GSE5900) (Figure 4C). Notably, patients with high *LILRB4* expression had significantly worse prognosis in both the

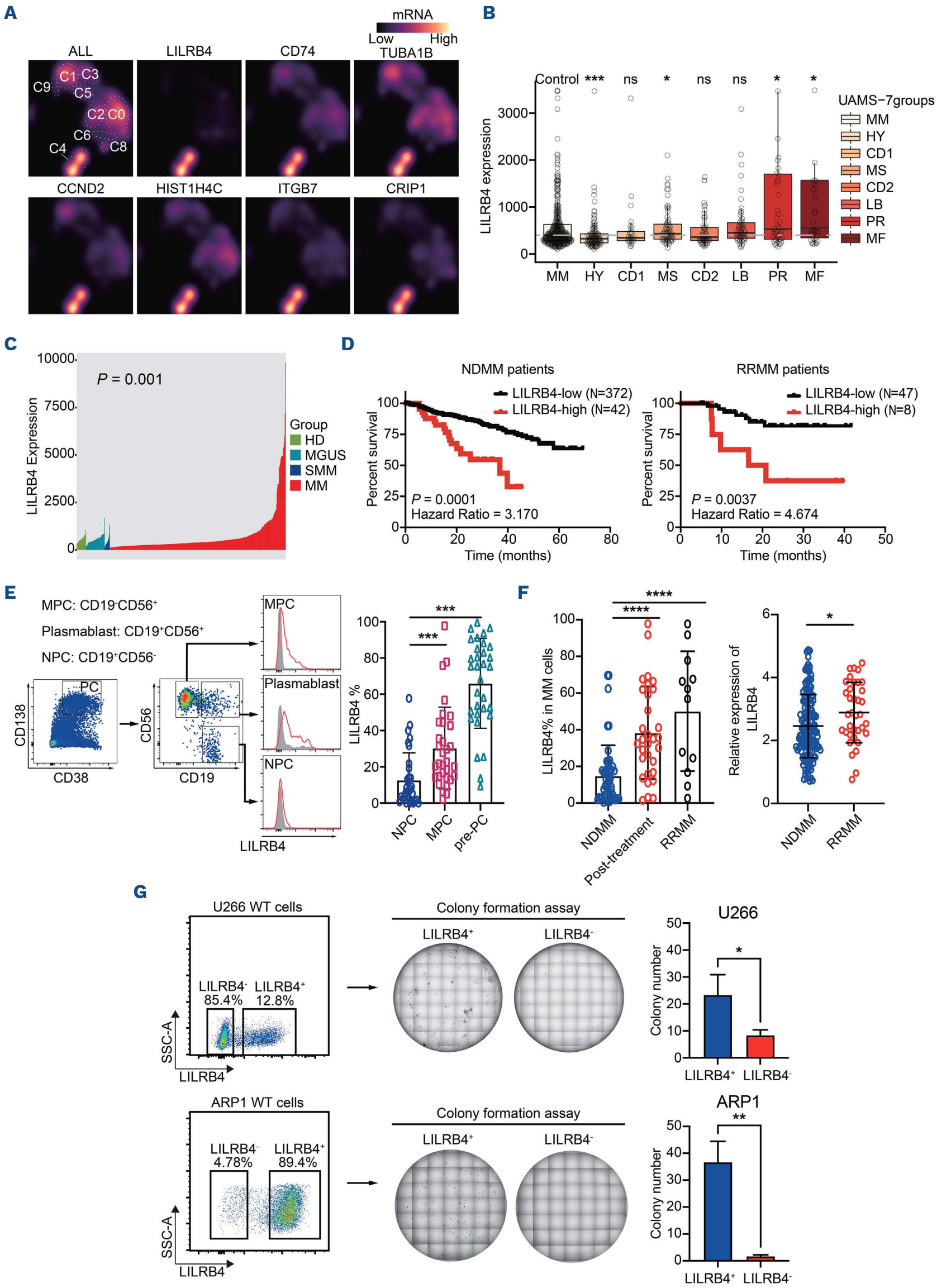

Continued on following page.

Figure 4. The expression pattern of the top gene, *LILRB4*, in multiple myeloma cells. (A) Fitted density plots illustrating the expression of seven specific genes in plasma cells selected by the lasso regression. algorithm. (B) Bar chart showing the expression of *LILRB4* in UAMS-7. (C) Bar plot illustrating *LILRB4* expression in healthy individuals and patients with monoclonal gammopathy of undetermined significance, smoldering multiple myeloma or multiple myeloma (MM). (D) Kaplan-Meier curve showing the overall survival of newly diagnosed MM (NDMM) patients (left panel, GSE2658) and relapsed/refractory MM (RRMM) patients (right panel, GSE57317) with high or low expression of *LILRB4*. A log-rank test was applied in the comparison between groups. (E) Left and middle. Density dot plots and line charts of flow cytometry analysis displaying the expression of LILRB4 protein in the population of plasma cells, malignant plasma cells, pre-plasma cells, and normal plasma cells from bone marrow aspirates of NDMM and RRMM patients. Right. Bar plot showing the statistical differences between different plasma-cell populations. Unpaired *t* test, ***P<0.001. (F) Left. Bar plot showing the percentage LILRB4 expression, detected by flow cytometry, in MM cells in NDMM patients (N=49), in MM patients after treatment (N=31), and in RRMM patients (N=12). Right. Dot plot showing mRNA expression of *LILRB4* in NDMM and RRMM patients. Unpaired *t* test, *P<0.05, ****P<0.0001. (G) Density dot plots of flow cytometry analysis displaying LILRB4$^+$ and LILRB4$^-$ MM cells. Optical microscope images showing the colony formation assay of LILRB4$^+$ and LILRB4$^-$ cells (5X magnification). Unpaired *t* test, *P<0.05, **P<0.01. UAMS: University of Arkansas Medical School; MM: multiple myeloma; HY: hyperdiploid; CD1: spiked CCND1/CCND3 expression; MS: spiked MMSET expression; CD2: spiked CCND1/CCND3 expression; LB: low bone disease; PR: proliferation; MF: MAF/MAFB spikes; HD: healthy donors; MGUS: monoclonal gammopathy of undetermined significance; SMM: smoldering multiple myeloma; MPC: malignant plasma cells; NPC: normal plasma cells; pre-PC: pre-plasma cells; WT: wild-type.

NDMM (GSE2658) and RRMM (GSE57317) cohorts (Figure 4D). These clinical data further support the concept that LILRB4 plays a critical role in the aggressive behavior of MM cells, resulting in the inferior outcome of patients.

Next, we confirmed the expression of *LILRB4* by measuring protein levels in MM/plasma cells from MM patients by flow cytometry. We observed that the level of ILT3, the protein encoded for by *LILRB4*, was significantly higher in the precursor stage of plasma cells (CD38$^+$CD138$^+$CD19$^+$CD56$^+$) than in mature malignant plasma cells (CD38$^+$CD138$^+$CD19$^-$CD56$^+$),

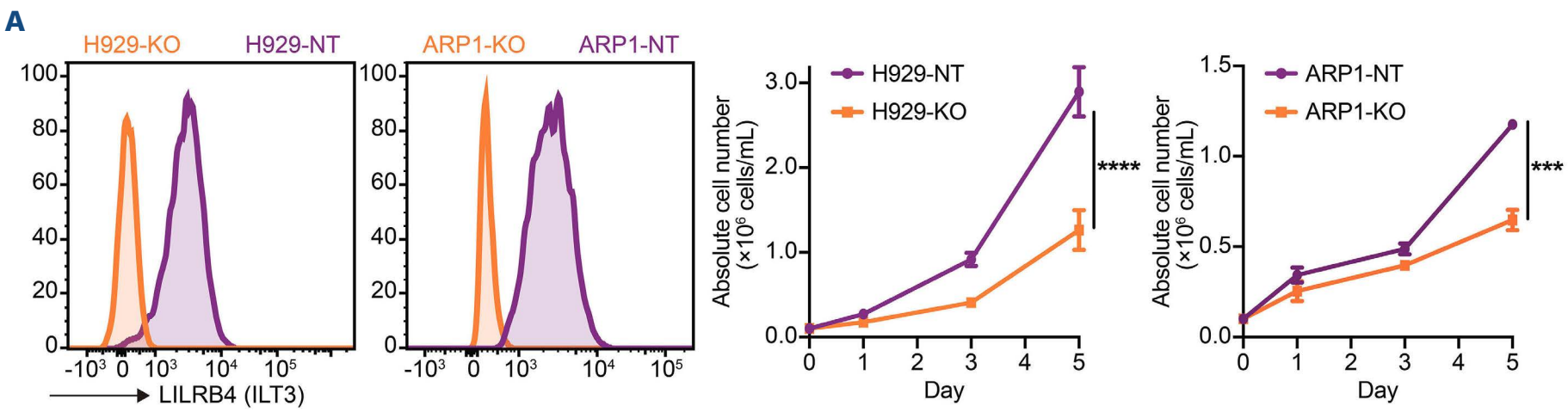

Continued on following page.

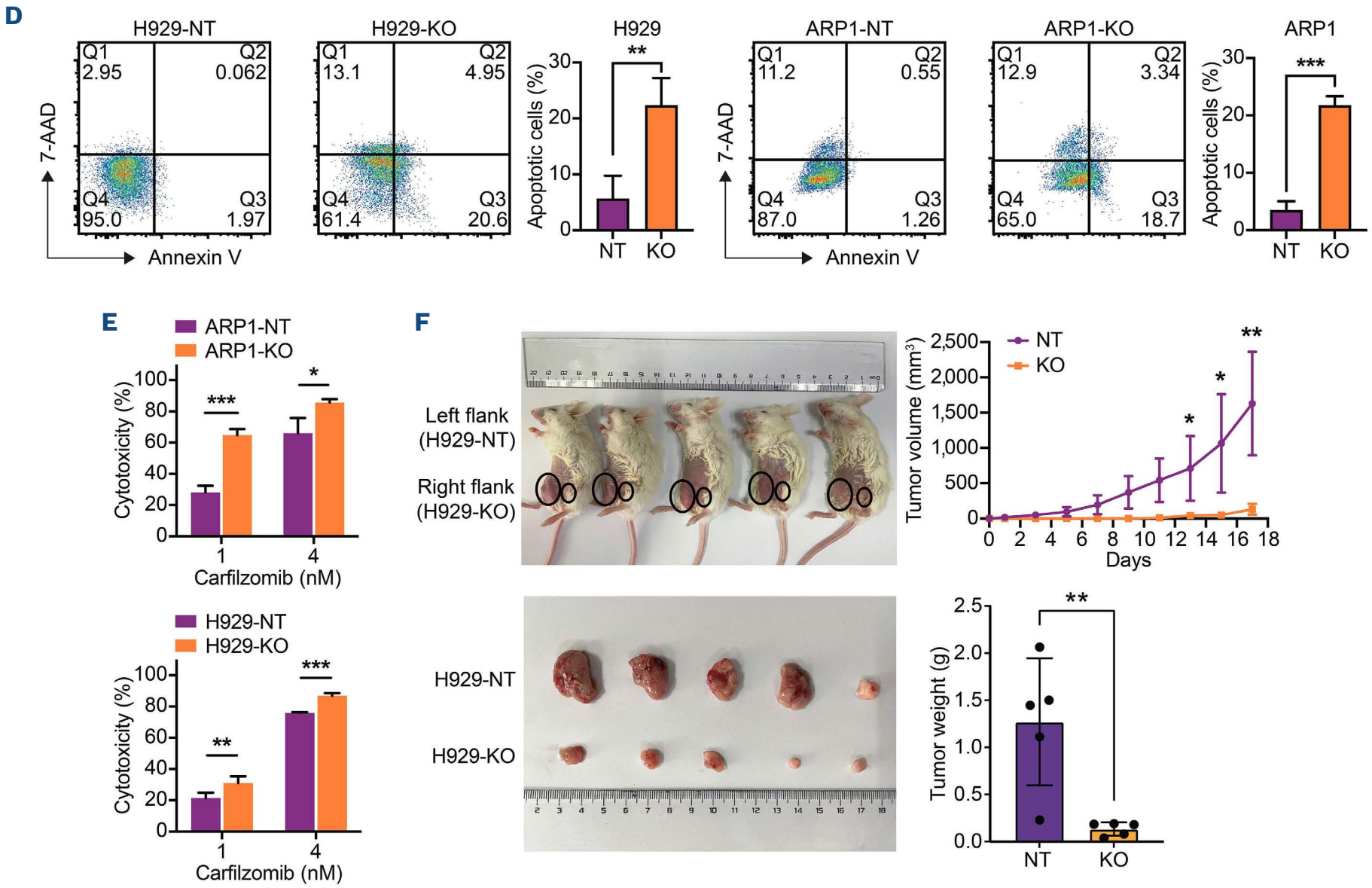

Figure 5. LILRB4 plays faceted roles in the progression of multiple myeloma. (A) Left. Flow cytometry detection of LILRB4 in non-target (NT) and *LILRB4* knock-out (KO) multiple myeloma (MM) cells. Right. Growth of *LILRB4*-KO cells relative to NT MM cells. (B) Colony formation assay of *LILRB4*-KO cells relative to NT MM cells (5X magnification). (C) Transwell invasion assay of *LILRB4*-KO cells relative to NT MM cells. (D) Cellular apoptosis detection of NT cells and LILRB4-KO MM cells. (E) Bar chart showing cytotoxicity towards NT cells and *LILRB4*-KO MM cells by carfilzomib at 48 h. (F) The H929-NT and H929-KO cells were injected subcutaneously into the left and right flank of the same mouse. A line plot showing the measurement of tumor volume every other day between H929-NT and H929-KO groups. Bar graphs showing the statistical difference of tumor weight between animals in the H929-NT and H929-KO groups. Unpaired *t* test, **P*<0.05, ***P*<0.01, ****P*<0.001, *****P*<0.0001.

and in both cases these levels were higher than those in normal plasma cells ($CD38^+CD138^+CD19^+CD56^-$) (Figure 4E). Minimal residual disease is the term used to describe a small number of cancer cells left in the body after treatment. These cells have the potential to multiply and cause relapses in patients. Of note, we found that the level of *LILRB4* was increased in residual MM cells after treatment compared with the level in NDMM cells (Figure 4F). Consistently, *LILRB4* level was further increased, at both transcriptional and protein levels, in RRMM patients (Figure 4F). In the MMRF-CoMMpass dataset, $LILRB4^{high}$ patients had higher drug-resistance and proliferation scores than $LILRB4^{low}$ patients, suggesting the possible involvement of *LILRB4* in aggressive behavior of MM cells (*Online Supplementary Figure S5B*). To further investigate the biological features of *LILRB4*, we first sorted LILRB4-positive and -negative cells in MM cell lines (*Online Supplementary Figure S5C, D*). Our data showed that endogenous LILRB4 promoted colony formation of MM cells (Figure 4G).

We also utilized CRISPR-Cas9 technology to genetically delete *LILRB4* from MM cell lines (H929 and ARP1) to detect the effects of LILRB4 in myelomagenesis. Deletion of *LILRB4* significantly suppressed the tumor growth and colony formation of MM cells (Figure 5A, B). Additionally, *LILRB4* knockout suppressed MM cell migration, promoted cell apoptosis, and increased the susceptibility of the MM cells to proteasome inhibitors (Figure 5C-E). Furthermore, the *in vivo* study demonstrated that tumor growth in *LILRB4*-KO group significantly decreased compared with that in the control animals (Figure 5F). Consistently, overexpression of *LILRB4* in H929 cells notably promoted colony formation and tumor growth *in vivo* (*Online Supplementary Figure S5E*, F). Collectively, the highly specific gene of the aggressive sub-C4 in MM cells, *LILRB4*, was a promising biomarker of aggressive MM cells which promoted MM clonogenicity and disease progression.

Next, we aimed to investigate the underlying molecular mechanisms of high *LILRB4* expression in MM cells. Based on the data shown in Figure 3B, amp(19) was one of the cytogenetic abnormalities in MM cells of sub-C4 and was the chromosome in which *LILRB4* was located. We, therefore, performed an assay for transposase-accessible chromatin using sequencing (ATAC sequencing) first. The results demonstrated that MM cell lines with a high level of *LILRB4* retained higher chromosomal accessibility in the *LILRB4* promoter region compared with *LILRB4* low-expressing MM cells (Figure 6A). According to the data shown in Figure 2E, the further analysis displayed significant H3K27ac enrichment in the *LILRB4* promoter region in seven of ten patients (*Online Supplementary Table S2*). To further explore the potential transcription factors that might regulate *LILRB4* expression, we used the hTFtarget human transcription factors ChIP-sequencing database (*http://bioinfo.life.hust.edu.cn/hTFtarget/*) and found that the transcription factor STAT1 could bind significantly to the *LILRB4* promoter region. The STAT1 ChIP-sequencing reads were enriched in the *LILRB4* promoter region (Figure 6B). Next, we treated MM cells with a STAT1-specific inhibitor, fludarabine. Inhibition of STAT1 significantly downregulated *LILRB4* expression in MM cells (Figure 6C). Of note, we co-cultured MM cells with microenvironment immune cells. We found that microenvironment cells could promote *LILRB4* expression in MM cells (Figure 6D).

LILRB4 plays a critical role in the immunosuppressive tumor microenvironment in multiple myeloma

As the previous study showed, LILRB4 is an immune checkpoint on myeloid cells.[37] Apart from its function in promoting aggressive progression of MM cells, as indicated by the data above, we were curious about whether high-level LILRB4 plays a critical role in the immunosuppressive TME in MM. We, therefore, downloaded the scRNA-sequencing data of pan-cancer myeloid cells from 45 human samples in a publicly available dataset and constructed a reference map using the STACAS package. Myeloid cell clusters were defined as four major lineages (mast cells, dendritic cells [DC], monocytes, or macrophages) based on canonical gene markers. DC were further identified as three distinct subsets, including two classical DC subsets (CLEC9A$^+$ cDC1 and CD1C$^+$ cDC2) and a mature classical DC subset (LAMP3$^+$ cDC). Monocytes were clustered into classical CD14^{hi}CD16$^-$ monocytes (Mono-CD14), intermediate CD14^{hi}CD16$^+$ monocytes (Mono-CD14CD16), and non-classical CD14$^+$ CD16^{hi} monocytes (Mono-CD16). Interestingly, we defined MDSC by high expression of CD33, ITGAM, and CCR2. Likewise, macrophage subsets were clustered into four subsets by specific high expression of C1QC, INHBA, LYVE1, and NLRP3 (*Online Supplementary Figure S6A-D*). We then projected the myeloid cells in the TME of our scRNA-sequencing data onto the reference map (Figure 7A, B; *Online Supplementary Figure S6E*).

Significantly elevated proportions of MDSC, Macro-C1QC, pDC-LILRA4, and Mono-CD16 were observed in EM24 patients according to fold changes in their proportions (Figure 7C). Of note, MDSC were validated to present preferential expression of genes involved in immune suppression (Figure 7D). Consistently, Macro-C1QC tended to be in a tumor-promoting M2 polarization state, while Macro-NLRP3 exhibited higher canonical M1 signatures. Among four DC clusters, pDC-LILRA4, which has been revealed to play a promoting role in MM progression, got the lowest activating and migratory score. In the monocyte compartment, CD16$^+$ monocytes tended to be anti-inflammatory, while CD14$^+$ monocytes and intermediate CD14^{hi}CD16$^+$ monocytes tended to be pro-inflammatory (Figure 7D). The results suggested that different types of myeloid cells in EM24 MM patients contributed to the severe immunosuppressive TME.

Given the specific *LILRB4*$^+$ sub-C4 of tumor cells enriched in EM24 patients and the cancer cell-to-TME communication, we characterized the phenotype of MDSC generated by co-culture of healthy human peripheral blood mononuclear cells *In vitro* with MM cells overexpressing *LILRB4* or control MM cells transduced with an empty vector. The co-culture of *LILRB4*-overexpressing MM cells induced generation of more monocytic MDSC (M-MDSC: CD15$^-$CD14$^+$) compared with co-culture with the empty vector control cells. *Vice versa*, deletion of *LILRB4* in MM cells mitigated the generation of MDSC from peripheral blood mononuclear cells (Figure 7E). However, we did not find the induction of granulocytic MDSC (G-MDSC; CD15$^+$CD14$^-$) in the co-culture assay (*data not shown*). Of note, in the co-culture system, the more MDSC induced by overexpression of *LILRB4* in MM cells promoted a greater decrease of CD3$^+$ T-cell infiltration, and knock-out of *LILRB4* in MM cells also increased T-cell infiltration (Figure 7E; *Online Supplementary Figure S6F*). Consistently, we noted decreased infiltration of MDSC in a myeloma mouse model that harbored *LILRB4*-KO tumor cells compared with non-target ones (Figure 7F). In summary, the infiltration of MDSC was efficiently induced by the enriched *LILRB4*$^+$ MM cells in EM24 patients. This finding further supports the concept that *LILRB4* promoted the generation of MM-educated M-MDSC, which contributed to the immunosuppressive TME and MM progression.

LILRB4 is a promising immunotherapy target via dual targeting of tumor cells and myeloid-derived suppressive cells in the tumor microenvironment of multiple myeloma

Besides MM cells, flow cytometry analysis confirmed that M-MDSC expressed high levels of LILRB4 (ILT3) compared with G-MDSC in samples from MM patients (Figure 8A). Given that LILRB4 is a surface marker on myeloma cells as well as MDSC, we speculated that LILRB4 could be an attractive immunotherapy target in MM therapy, especially in patients with RRMM. Strikingly, we constructed a STAR-T cell targeting cells positive for LILRB4, a double-chain chimeric receptor,

which incorporates an antigen-recognition domain of antibody and constant regions of TCR that engage the endogenous CD3 signaling machinery (*Online Supplementary Figure S7A*).[22,38] We investigated the cytotoxicity of LILRB4 STAR-T-cell immunotherapy utilizing MM cell lines, a xenograft MM mouse model and primary patients' samples. LILRB4 STAR-T cells or mock-T cells were co-cultured with MM cell lines, H929 and U266, at various effector:target (E:T) ratios. Compared with mock-T cells, LILRB4 STAR-T cells showed strong cytotoxicity against MM cell lines, and secreted high levels of cytokines including interferon-γ, interleukin-2, and tumor necrosis factor-α (Figure 8B). LILRB4 STAR-T cells had no obvious cytotoxicity towards LILRB4-negative cells, indicating limited off-target effects (*Online Supplementary Figure S7B*). The *in vivo* study was further performed in an MM xenograft model with subcutaneous injection of H929 cells. Consistently, compared with treatment with mock-T cells, LILRB4 STAR-T-cell immunotherapy exhibited rapid and strong anti-MM activity (Figure 8C). The survival of MM-bearing mice was significantly extended compared with that of the control group (undefined *vs*. 30 days) (Figure 8C). Importantly, we did not find obvious off-tumor toxicity, as shown by weight and histochemical staining data (*Online Supplementary Figure S7C, D*).

To investigate the cytotoxicity of LILRB4 STAR-T cells against MDSC, we purified $CD14^+$ monocytes from healthy peripheral blood mononuclear cells that were used to generate M-MDSC by adding a cocktail of cytokines (Figure 8D).[39] These M-MDSC were then co-cultured with mock-T cells or LILRB4 STAR-T cells. Specific lysis and interferon-γ cytokine secretion were significantly increased in the group treated with LILRB4 STAR-T cells (Figure 8D). As B-cell maturation antige (BCMA) has been a successful immunotherapy target in MM, we investigated the association between BCMA and LILRB4 expression. We found that LILRB4 level was independent of BCMA based on the GSE2658 dataset (r=0.04, *P*=0.28). and that the expression of BCMA protein was not significantly altered in LILRB4-overexpressing MM cell lines (*Online Supplementary Figure S7E*). Furthermore, primary BMMC from MM patients,

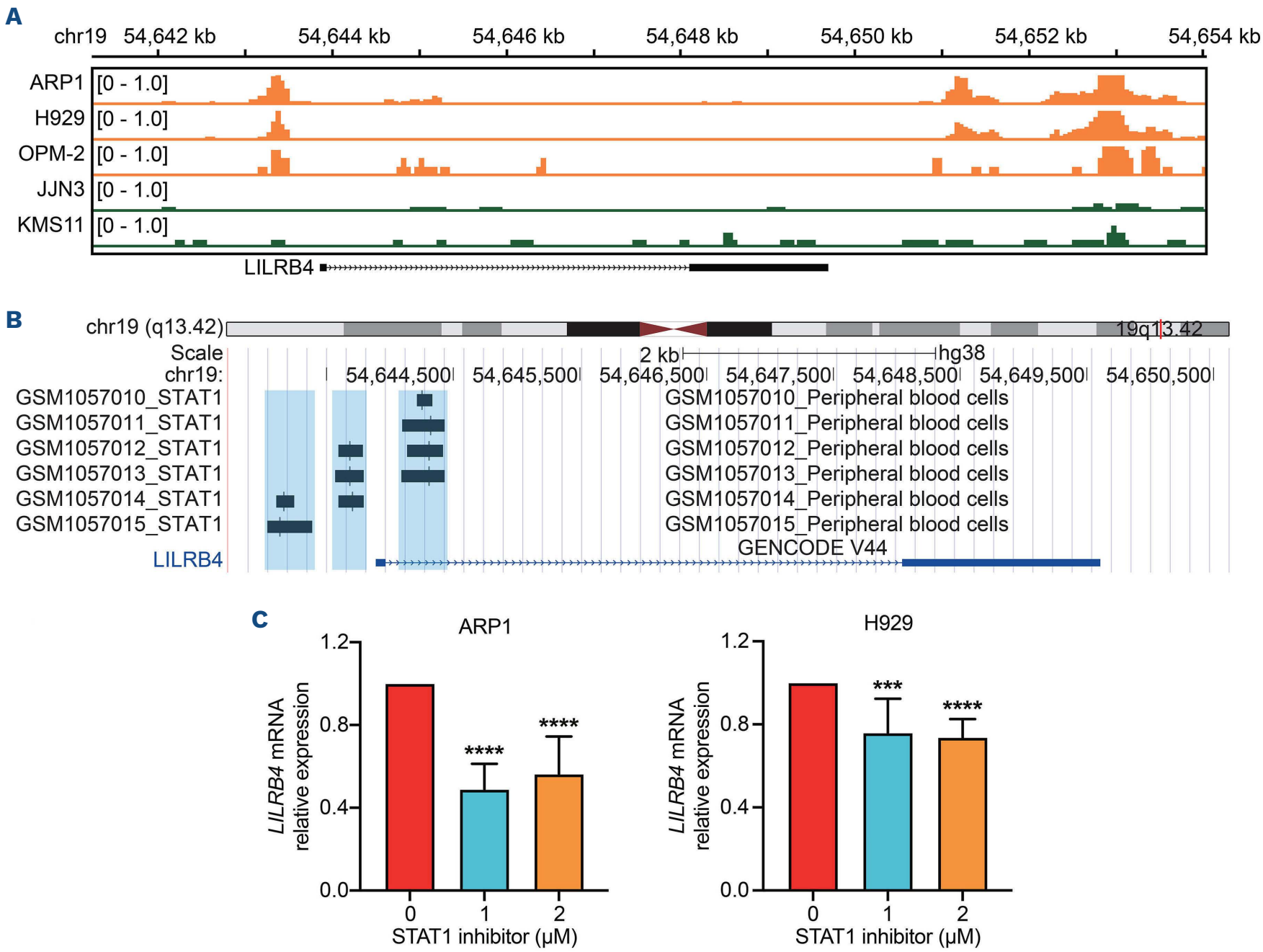

Continued on following page.

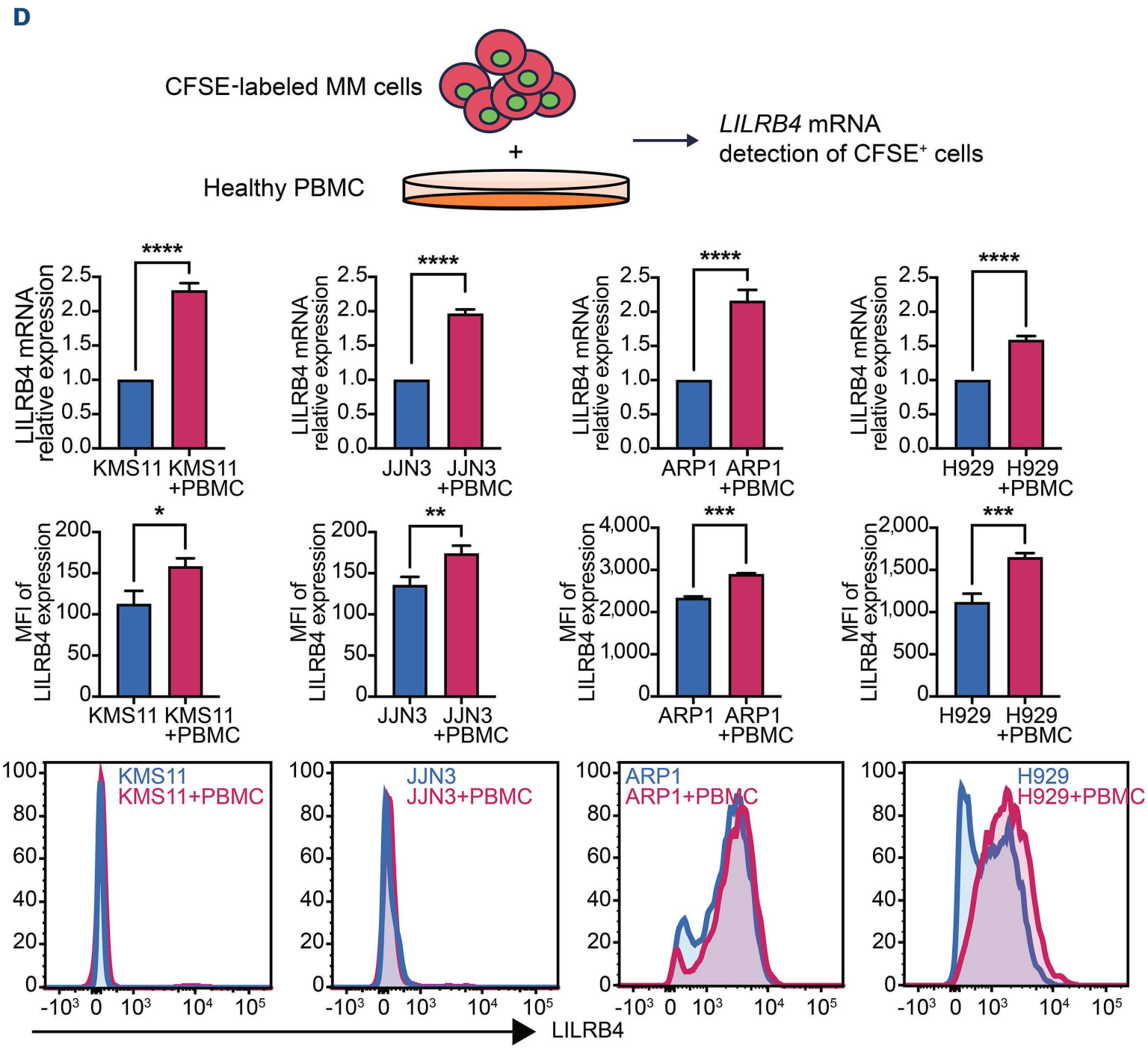

Figure 6. The regulated mechanisms underlying LILRB4 expression in multiple myeloma cells. (A) ATAC-sequencing unveiling a significant increase in chromatin accessibility within the promoter region of the *LILRB4* gene in multiple myeloma (MM) cell lines exhibiting elevated expression levels of LILRB4. (B) STAT1 ChIP-sequencing reads enriched in the *LILRB4* promoter region. (C) *LILRB4* mRNA expression in MM cells treated with the STAT1 inhibitor, fludarabine, for 48 h. (D) Top. Schematic diagram showing the experimental process of MM cells co-cultured with healthy peripheral blood mononuclear cells for 72 h. Middle. The bar charts show *LILRB4* mRNA expression and LILRB4 mean fluorescence intensity in MM cells after co-culture. Bottom. The histograms show the flow cytometry examination of LILRB4 in MM cells after co-culture. CFSE: carboxyfluorescein succinimidyl ester; PBMC: peripheral blood mononuclear cells; MFI: mean fluorescence intensity.

including patients receiving or not receiving BCMA-targeted immunotherapy, were isolated and treated with LILRB4 STAR-T cells at various E:T ratios (*Online Supplementary Table S3*). Based on our data described above (Figures 2F and 4E), we confirmed that CD38^{+}LILRB4^{+} cells included CD38^{+}LILRB4^{+}CD138^{high} and CD38^{+}LILRB4^{+}CD138^{low} cell clusters in almost every MM patient. Since CD38^{+}CD138^{high} is suggested to be the conventional surface marker for MM cells, we further utilized light chain restriction analysis and validated that the CD38^{+}CD138^{low}LILRB4^{+} cell cluster contained the clonogenic MM tumor cells (*Online Supplementary Figure S7F*). Strikingly, treatment with LILRB4 STAR-T cells exhibited obvious cytotoxicity against both CD38^{+}LILRB4^{+} MM cells and CD11b^{+}LILRB4^{+} M-MDSC from patients who had received BCMA CAR-T therapy (Figure 8E). Altogether, our study strongly supports that targeting *LILRB4* is a promising immunotherapy strategy by dual targeting MM cells and immunosuppressive MDSC in the TME of MM.

Discussion

Although long-term disease control can be achieved in a very large number of patients with MM, the acquisition of tumor resistance leads to disease relapse, especially

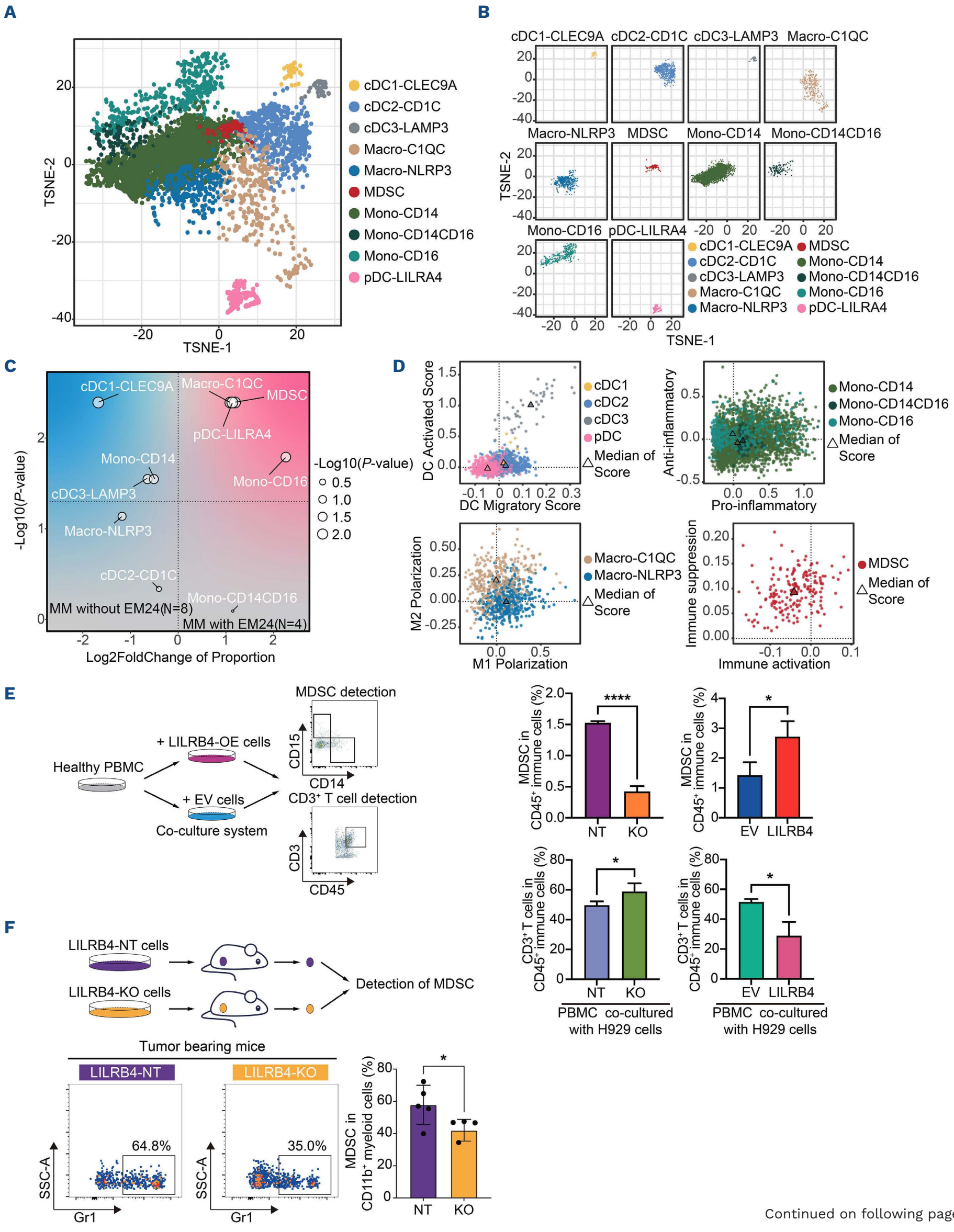

Continued on following page.

Figure 7. High infiltration of immunosuppressive myeloid cells in EM24 multiple myeloma patients. (A) T-distributed stochastic neighbor embedding (TSNE) plots showing the distribution of annotated myeloid cells. Cell annotations are labeled by colors. (B) TSNE plots showing the marker gene expression of each cell cluster. (C) Point plot displaying changes in myeloid cell composition between patients who died early (early mortality within 24 months; EM24) and patients without early death (nEM24). For each cell type, two axes indicate the log fold change in mean cell fraction between the two groups, with $-\log_{10}$ two-sided Wilcoxon rank sum *P* values. (D) Scatterplots showing dendritic cell migratory and activated scores (top left), pro- and anti-inflammatory scores (top right), M1 and M2 polarization scores (bottom left), and immune activation and suppression scores (bottom right) for colored myeloid cell types. Triangles represent the median of the cell scores. (E) Left. Schematic diagram showing the experimental procedure. Multiple myeloma (MM) cells were co-cultured with peripheral blood mononuclear cells (PBMC) from healthy donors and then the differentiation of myeloid-derived suppressive cells (MDSC) and T-cell proportion were measured. Right. Bar charts showing the proportion of MDSC and $CD3^+$ T cells in PBMC after co-culture with H929 MM cells with different LILRB4 levels. Statistical analysis using a two-tailed unpaired Student *t* test, $*P<0.05$, $****P<0.0001$. (F) Top left. Schematic diagram of the experimental procedure. Non-target (NT) and LILRB4 knock-out (KO) H929 cells were injected subcutaneously into the mice, followed by detection of infiltrated MDSC in tumor samples. Bottom left. Density dot plots displaying the MDSC population in the NT and KO groups. Right. Bar chart showing the proportion of MDSC in myeloid cells between the NT and LILRB4-KO groups. Statistical analysis using a two-tailed unpaired Student *t* test, $*P<0.05$.

in patients with triple-class refractory MM (defined as resistance to immunomodulatory agents, proteasome inhibitors, and monoclonal antibodies). There is an unmet need for effective treatment options in these patients. CAR-T-cell therapy is a novel approach that has demonstrated promising efficacy in the treatment of RRMM. The interaction and co-evolution of tumor cells and their microenvironment are among the principal causes of MM refractoriness.[14] Thus, simultaneously eliminating tumor cells and ameliorating the TME to achieve minimal residual

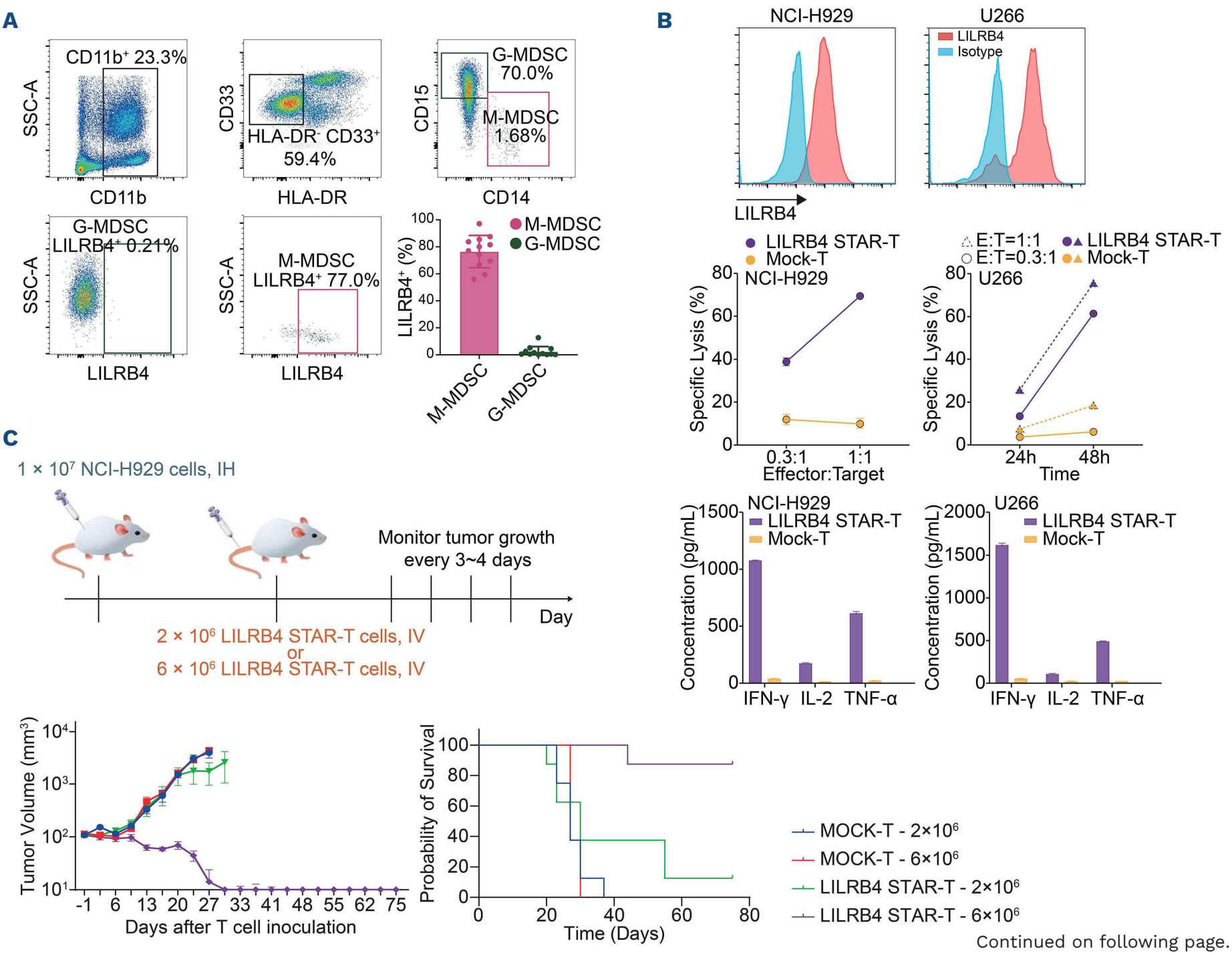

Continued on following page.

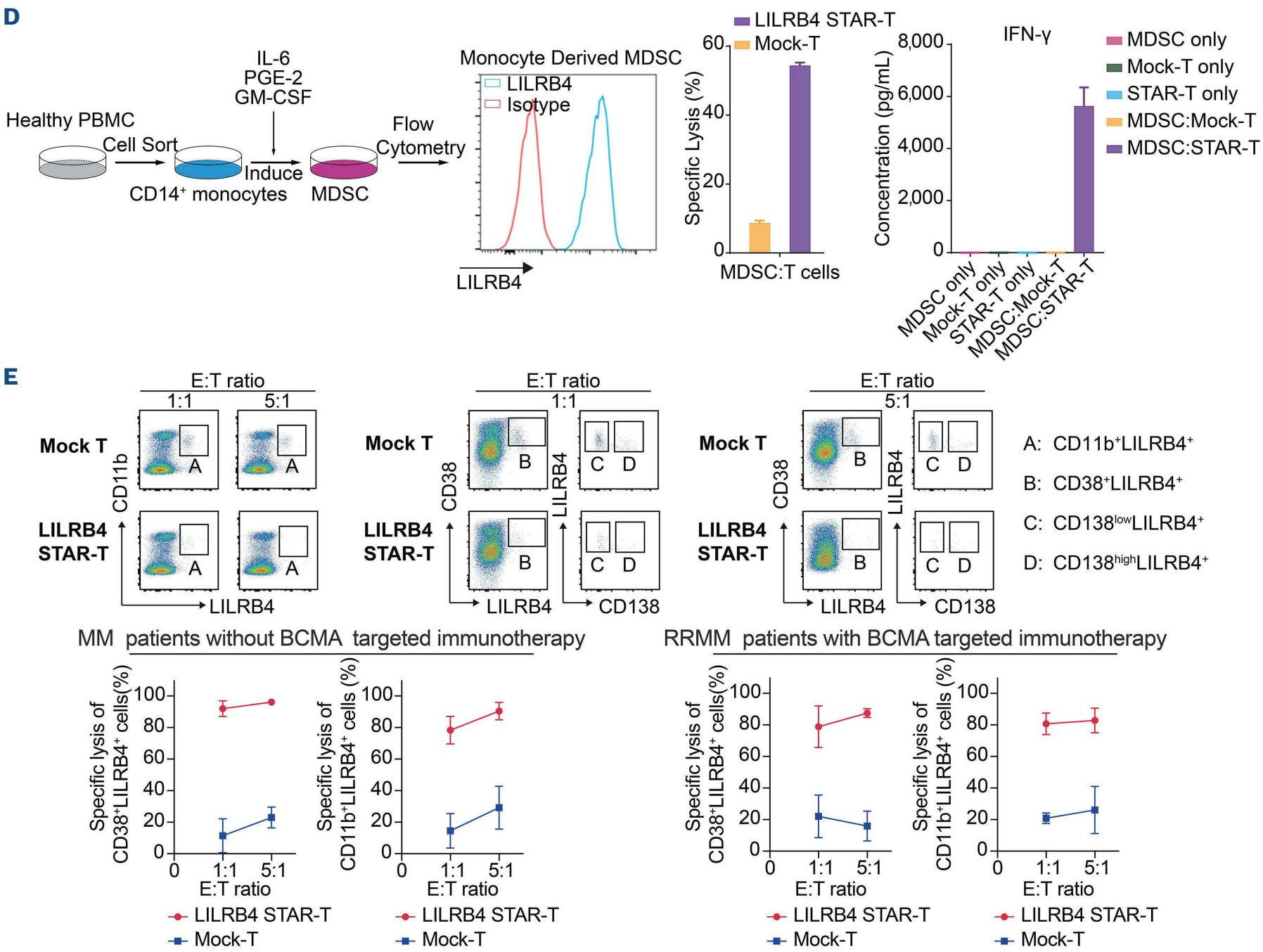

Figure 8. LILRB4 is a promising target for immunotherapy of multiple myeloma. (A) Density dot plots of flow cytometry analysis displaying the expression of LILRB4 protein in the population of monocytic myeloid-derived suppressive cells (M-MDSC) and granulocytic myeloid-derived suppressive cells (G-MDSC) from patients with multiple myeloma (MM). Strategies for gating are shown in the figure. Bottom right. Bar chart showing the expression of LILRB4 protein in M-MDSC and G-MDSC. (B) Top. Density line charts of the flow cytometry analysis displaying the expression of LILRB4 protein in NCI-H929 and U266 MM cells. Middle. Point plots showing the percentages of cell lysis of NCI-H929 and U266 MM cells co-cultured with mock-T cells (yellow) or LILRB4-targeted synthetic T-cell receptor and antigen receptor (STAR)-T cells (purple) under different effector:target (E:T) ratios and for different periods of incubation (middle panel). Bottom. Bar charts showing the concentration of interferon-γ, interleukin-2, and tumor necrosis factor-α secreted by T cells after co-culture. (C) Top. Schematic of the monitoring of the anti-tumor function of LILRB4 STAR-T cells in a xenograft tumor model. Bottom left. Line charts illustrating the subcutaneous tumor volume in MM xenograft mice after treating mock-T cells or LILRB4-targeted STAR-T cells. The mean tumor volumes with standard error bars were calculated on specific days. Bottom right. Kaplan-Meier curve showing the survival of the MM xenografted mice. (D) Left. Experimental design. Middle. Density line charts of flow cytometry analysis displaying the expression of LILRB4 protein in M-MDSC. Right. Bar charts showing the percentage of cell lysis M-MDSC co-cultured with mock-T cells or LILRB4-targeted STAR-T cells and the concentration of interferon-γ, IL-2 after co-culture. (E) Exemplary dot plots obtained in the flow cytometry-based LILRB4 STAR-T cell cytotoxicity assay. Bone marrow mononuclear cells from MM patients (N=9) were co-cultured with LILRB4 STAR-T or mock-transduced T cells at different E:T ratios. After 4 hours of incubation, specific lysis of CD38⁺LILRB4⁺ cells and CD11b⁺LILRB4⁺ immunosuppressive myeloid cells by LILRB4 STAR-T or mock-transduced T cells was quantified and calculated by flow cytometry using counting beads.

disease-negativity is the ideal treatment strategy for MM. Our data here demonstrated enrichment of an *LILRB4*^{high} precursor plasma-cell cluster in ultrahigh-risk patients with overall survival of less than 2 years. This immature population of cells was closely correlated with aggressive progression and drug resistance of MM. Recently, high levels of *LILRB4* were detected in both MM cells and myeloid cells.[40-43] However, the clinical significance and the pathophysiological function of LILRB4 in MM has not been fully understood. LILRB4, an immune checkpoint

on myeloid cells, has been validated to be an effective treatment target in monocytic acute myeloid leukemia and mediates acute myeloid leukemia cell migration and T-cell suppression.[40] Recently, Qu *et al.* reported that LILRB4 could promote MM cell migration and was upregulated in extramedullary MM cells.[44] Here, we demonstrated that LILRB4 plays multifaceted roles in promoting MM. High levels of *LILRB4* promoted the clonogenicity of MM cells. Deletion of *LILRB4* efficiently alleviated tumor growth, mitigated cell migration, promoted cell apoptosis, and increased the susceptibility to proteasome inhibitors in MM cells. Importantly, our study identified that chromosomal accessibility and H3K27ac enrichment promoted *LILRB4* gene transcription. Most interestingly, we indicated that the TME could interact with MM cells and upregulate the expression of LILRB4 in tumor cells. The regulatory mechanism might involve direct or indirect cell contact. As our previous studies indicated, the interaction between microenvironment cells could be accomplished by secreted cytokines, microvesicles, or cellular metabolites.[16,45,46] The precise mechanisms of LILRB4 expression regulation by the TME needs to be explored further. Generally, our results indicate that the mechanisms underlying the regulation of LILRB4 expression are very complex and involve various factors and processes.

MDSC are an important component of the immunosuppressive TME and play supportive roles in cancer.[47,48] Interestingly, co-culture of *LILRB4*^{high} MM cells orchestrated the polarization of MDSC to exhibit pro-tumor phenotypes. This added further support to the understanding that the abundant MDSC in EM24 MM patients induce a more severe immunosuppressive microenvironment. Therefore, our result suggest that *LILRB4*, the most significantly highly expressed gene in the pre-mature MM population, is an attractive immunotherapy candidate target for curing MM through targeting both tumor cells and the immunosuppressive TME, especially in ultrahigh-risk NDMM and RRMM patients.

Among many targets of MM immunotherapy, BCMA and orphan G protein-coupled receptor, class C group 5 member D (GPRC5D) are the most successful and mature targets. CAR-T-cell therapy and bispecific T-cell engagers targeting BCMA or GPRC5D have significantly improved responses to treatment and survival of RRMM patients.[49,50] However, the long-term follow-up of current studies has indicated limited short-term efficacy of CAR-T-cell therapy for RRMM.[51] The mechanisms underlying resistance to T-cell-based immunotherapy are complicated. BCMA and GPRC5D are mainly expressed on mature plasma cells and MM cells.[52,53] Current immunotherapy mostly targets mature plasma cells and is incapable of eliminating pre-mature plasma cells or pre-B cells that do not express the target antigens, which may lead to disease relapse and progression.[54-56] In addition, the immunosuppressive TME, including MDSC, can affect the efficacy of T-cell-based immunotherapy. Our data indicated high expression of *LILRB4* in plasmablasts, mature MM cells, and MDSC, suggesting the feasibility of LILRB4-targeted immunotherapy in MM. Considering our findings collectively, we suppose that targeting LILRB4 could eradicate potential tumor-initiating cells and impede MDSC as well as enhance the antitumor effect of T-cell therapy. Based on this concept, our group designed and constructed innovative LILRB4-targeted STAR-T cells, which incorporate the antigen-recognition domain of antibodies and constant regions of TCR that engage endogenous CD3 signaling machinery. STAR-T cells can mediate strong and sensitive TCR-like signaling upon antigen stimulation.[22] In addition, STAR-T cells have the potential to reduce the risk of antigen loss-induced tumor relapse due to the high antigen sensitivity. We demonstrated that LILRB4 STAR-T cells show excellent cytotoxicity against tumor cells and MDSC and extend the survival of myeloma-bearing mice. We did not find off-tumor cytotoxic effects *in vivo*. Recently a bispecific T-cell engager targeting LILRB4 has shown potent killing effects toward MM cells,[43] reinforcing the concept that LILRB4 is an attractive immunotherapy target with promising prospects for development and application. Based on this study, we have set up an investigator-initiated trial to explore the safety and efficacy of LILRB4 STAR-T cells in RRMM (Clinical Trial: NCT05913804). The feasibility and underlying mechanisms of LILRB4-STAR-T immunotherapy in MM is under further investigation.

In conclusion, our study delineated that LILRB4 is an ideal biomarker for the identification of high-risk MM, and represents a promising target for MM immunotherapeutics by dual targeting tumor cells and MDSC. Strikingly, our findings further suggested that combining LILRB4-STAR-T cell treatment with BCMA targeting therapy would be an attractive strategy for RRMM.

Disclosures

No conflicts of interest to disclose.

Contributions

LG and HS conducted experiments, acquired and analyzed data, and wrote the original draft. LLiu and LLei constructed the in vivo experiment. YL and XS contributed to the ATAC-sequencing and data analysis. TF, ZY, and FF collected and analyzed data. JX, WS, TW, and GA participated in collecting patients' samples and clinical data analysis. WR and XZ constructed the STAR-T. MH contributed to conceptualization, data curation, formal analysis, methodology, project administration, supervision, and editing. XL, LQ, and MH contributed to funding acquisition, investigation, and manuscript revision. All authors reviewed and approved the final version of the manuscript. The corresponding author attests that all listed authors meet authorship criteria and that no others meeting the criteria have been omitted.

Funding

This research was funded by the National Natural Science Foundation of China (82341211, 82370210, and 82170194) and the CAMS Innovation Fund for Medical Sciences (CIFMS 2022-I2M1-022 and CIFMS 2021-I2M1-040). The funder had no role in the study design, data collection, analysis, and interpretation, or in the writing of this manuscript.

Data-sharing statement

The in-house data presented in the study are deposited in the Genome Sequence Archive (GSA) repository (https://bigd.big.ac.cn/gsa-human/browse/HRA003504), BioProject ID: PRJCA013382, accession ID: HRA003504.

References

1. Bazarbachi AH, Al Hamed R, Malard F, et al. Relapsed refractory multiple myeloma: a comprehensive overview. Leukemia. 2019;33(10):2343-2357.
2. Kumar S, Baizer L, Callander NS, et al. Gaps and opportunities in the treatment of relapsed-refractory multiple myeloma: consensus recommendations of the NCI Multiple Myeloma Steering Committee. Blood Cancer J. 2022;12(6):98.
3. Cowan AJ, Green DJ, Kwok M, et al. Diagnosis and management of multiple myeloma: a review. JAMA. 2022;327(5):464-477.
4. Sonneveld P, Avet-Loiseau H, Lonial S, et al. Treatment of multiple myeloma with high-risk cytogenetics: a consensus of the International Myeloma Working Group. Blood. 2016;127(24):2955-2962.
5. Ríos-Tamayo R, Sáinz J, Martínez-López J, et al. Early mortality in multiple myeloma: the time-dependent impact of comorbidity: a population-based study in 621 real-life patients. Am J Hematol. 2016;91(7):700-704.
6. Terebelo H, Srinivasan S, Narang M, et al. Recognition of early mortality in multiple myeloma by a prediction matrix. Am J Hematol. 2017;92(9):915-923.
7. Neuse CJ, Lomas OC, Schliemann C, et al. Genome instability in multiple myeloma. Leukemia. 2020;34(11):2887-2897.
8. Tirier SM, Mallm JP, Steiger S, et al. Subclone-specific microenvironmental impact and drug response in refractory multiple myeloma revealed by single-cell transcriptomics. Nat Commun. 2021;12(1):6960.
9. Kumar SK, Rajkumar SV. The multiple myelomas - current concepts in cytogenetic classification and therapy. Nat Rev Clin Oncol. 2018;15(7):409-421.
10. Yan Y, Qin X, Liu J, et al. Clonal phylogeny and evolution of critical cytogenetic aberrations in multiple myeloma at single-cell level by QM-FISH. Blood Adv. 2022;6(2):441-451.
11. Pawlyn C, Morgan GJ. Evolutionary biology of high-risk multiple myeloma. Nat Rev Cancer. 2017;17(9):543-556.
12. Liu R, Gao Q, Foltz SM, et al. Co-evolution of tumor and immune cells during progression of multiple myeloma. Nat Commun. 2021;12(1):2559.
13. Dutta AK, Alberge JB, Sklavenitis-Pistofidis R, et al. Single-cell profiling of tumour evolution in multiple myeloma - opportunities for precision medicine. Nat Rev Clin Oncol. 2022;19(4):223-236.
14. Lv J, Sun H, Gong L, et al. Aberrant metabolic processes promote the immunosuppressive microenvironment in multiple myeloma. Front Immunol. 2022;13:1077768.
15. Zavidij O, Haradhvala NJ, Mouhieddine TH, et al. Single-cell RNA sequencing reveals compromised immune microenvironment in precursor stages of multiple myeloma. Nat Cancer. 2020;1(5):493-506.
16. Hao M, Zhang L, An G, et al. Suppressing miRNA-15a/-16 expression by interleukin-6 enhances drug-resistance in myeloma cells. J Hematol Oncol. 2011;4:37.
17. Hao M, Zhang L, An G, et al. Bone marrow stromal cells protect myeloma cells from bortezomib induced apoptosis by suppressing microRNA-15a expression. Leuk Lymphoma. 2011;52(9):1787-1794.
18. Sun H, Fang T, Wang T, et al. Single-cell profiles reveal tumor cell heterogeneity and immunosuppressive microenvironment in Waldenström macroglobulinemia. J Transl Med. 2022;20(1):576.
19. Jia Y, Zhou J, Tan TK, et al. Myeloma-specific superenhancers affect genes of biological and clinical relevance in myeloma. Blood Cancer J. 2021;11(2):32.
20. Agarwal P, Alzrigat M, Párraga AA, et al. Genome-wide profiling of histone H3 lysine 27 and lysine 4 trimethylation in multiple myeloma reveals the importance of Polycomb gene targeting and highlights EZH2 as a potential therapeutic target. Oncotarget. 2016;7(6):6809-6823.
21. Yu G, Wang LG, He QY. ChIPseeker: an R/Bioconductor package for ChIP peak annotation, comparison and visualization. Bioinformatics. 2015;31(14):2382-2383.
22. Liu Y, Liu G, Wang J, et al. Chimeric STAR receptors using TCR machinery mediate robust responses against solid tumors. Sci Transl Med. 2021;13(586):eabb5191.
23. An G, Xu Y, Shi L, et al. Chromosome 1q21 gains confer inferior outcomes in multiple myeloma treated with bortezomib but copy number variation and percentage of plasma cells involved have no additional prognostic value. Haematologica. 2014;99(2):353-359.
24. Rajkumar SV. Multiple myeloma: 2022 update on diagnosis, risk stratification, and management. Am J Hematol. 2022;97(8):1086-1107.
25. Liu L, Yu Z, Cheng H, et al. Multiple myeloma hinders erythropoiesis and causes anaemia owing to high levels of CCL3 in the bone marrow microenvironment. Sci Rep. 2020;10(1):20508.
26. Gao M, Bai H, Jethava, Y, et al. Identification and characterization of tumor-initiating cells in multiple myeloma. J Natl Cancer Inst. 2020;112(5):507-515.
27. Caron M, St-Onge P, Sontag T, et al. Single-cell analysis of childhood leukemia reveals a link between developmental states and ribosomal protein expression as a source of intra-individual heterogeneity. Sci Rep. 2020;10(1):8079.
28. Mehtonen J, Teppo S, Lahnalampi M, et al. Single cell characterization of B-lymphoid differentiation and leukemic cell states during chemotherapy in ETV6-RUNX1-positive pediatric leukemia identifies drug-targetable transcription factor activities. Genome Med. 2020;12(1):99.
29. Zhang Y, Wang S, Zhang J, et al. Elucidating minimal residual disease of paediatric B-cell acute lymphoblastic leukaemia by single-cell analysis. Nat Cell Biol. 2022;24(2):242-252.

30. Shaughnessy JD Jr., Zhan F, Burington BE, et al. A validated gene expression model of high-risk multiple myeloma is defined by deregulated expression of genes mapping to chromosome 1. Blood. 2007;109(6):2276-2284.
31. Zhou W, Yang Y, Xia J, et al. NEK2 induces drug resistance mainly through activation of efflux drug pumps and is associated with poor prognosis in myeloma and other cancers. Cancer Cell. 2013;23(1):48-62.
32. Hao M, Franqui-Machin R, Xu H, et al. NEK2 induces osteoclast differentiation and bone destruction via heparanase in multiple myeloma. Leukemia. 2017;31(7):1648-1650.
33. Franqui-Machin R, Hao M, Bai H, et al. Destabilizing NEK2 overcomes resistance to proteasome inhibition in multiple myeloma. J Clin Invest. 2018;128(7):2877-2893.
34. Kuiper R, Broyl A, de Knegt Y, et al. A gene expression signature for high-risk multiple myeloma. Leukemia. 2012;26(11):2406-2413.
35. Steiert B, Timmer J, Kreutz C. L1 regularization facilitates detection of cell type-specific parameters in dynamical systems. Bioinformatics. 2016;32(17):i718-i726.
36. Zhan F, Huang Y, Colla S, et al. The molecular classification of multiple myeloma. Blood. 2006;108(6):2020-2028.
37. Yang T, Qian Y, Liang X, et al. LILRB4, an immune checkpoint on myeloid cells. Blood Sci. 2022;4(2):49-56.
38. Wang J, Zhang X, Zhou Z, et al. A novel adoptive synthetic TCR and antigen receptor (STAR) T-cell therapy for B-cell acute lymphoblastic leukemia. Am J Hematol. 2022;97(8):992-1004.
39. Bancaro N, Calì B, Troiani M, et al. Apolipoprotein E induces pathogenic senescent-like myeloid cells in prostate cancer. Cancer Cell. 2023;41(3):602-619.
40. Deng M, Gui X, Kim J, et al. LILRB4 signalling in leukaemia cells mediates T cell suppression and tumour infiltration. Nature. 2018;562(7728):605-609.
41. Zurli V, Wimmer G, Cattaneo F, et al. Ectopic ILT3 controls BCR-dependent activation of Akt in B-cell chronic lymphocytic leukemia. Blood. 2017;130(18):2006-2017.
42. Li J, Gao A, Zhang F, et al. ILT3 promotes tumor cell motility and angiogenesis in non-small cell lung cancer. Cancer Lett. 2021;501:263-276.
43. Di Meo F, Iyer A, Akama K, et al. A target discovery pipeline identified ILT3 as a target for immunotherapy of multiple myeloma. Cell Rep Med. 2023;4(7):101110.
44. Sun Z, Ji J, Li Y, et al. Identification of evolutionary mechanisms of myelomatous effusion by single-cell RNA sequencing. Blood Adv. 2023;7(15):4148-4159.
45. Yu T, Du C, Ma X, et al. Polycomb-like protein 3 induces proliferation and drug resistance in multiple myeloma and is regulated by miRNA-15a. Mol Cancer Res. 2020;18(7):1063-1073.
46. Wei X, Yu Z, Tang P, et al. Multiple myeloma-derived miR-27b-3p facilitates tumour progression via promoting tumour cell proliferation and immunosuppressive microenvironment. Clin Transl Med. 2023;13(1):e1140.
47. Li K, Shi H, Zhang B, et al. Myeloid-derived suppressor cells as immunosuppressive regulators and therapeutic targets in cancer. Signal Transduct Target Ther. 2021;6(1):362.
48. Veglia F, Sanseviero E, Gabrilovich DI. Myeloid-derived suppressor cells in the era of increasing myeloid cell diversity. Nat Rev Immunol. 2021;21(8):485-498.
49. Wang D, Wang J, Hu G, et al. A phase 1 study of a novel fully human BCMA-targeting CAR (CT103A) in patients with relapsed/refractory multiple myeloma. Blood. 2021;137(21):2890-2901.
50. Mailankody S, Devlin SM, Landa J, et al. GPRC5D-targeted CAR T cells for myeloma. N Engl J Med. 2022;387(13):1196-1206.
51. Lee LSH, Yong KL. BCMA CARs in multiple myeloma: room for more? Blood. 2021;137(21):2859-2860.
52. van de Donk N, Usmani SZ, Yong K. CAR T-cell therapy for multiple myeloma: state of the art and prospects. Lancet Haematol. 2021;8(6):e446-e461.
53. Cappell KM, Kochenderfer JN. Long-term outcomes following CAR T cell therapy: what we know so far. Nat Rev Clin Oncol. 2023;20(6):359-371.
54. Raje N, Berdeja J, Lin Y, et al. Anti-BCMA CAR T-cell therapy bb2121 in relapsed or refractory multiple myeloma. N Engl J Med. 2019;380(18):1726-1737.
55. Smith EL, Harrington K, Staehr M, et al. GPRC5D is a target for the immunotherapy of multiple myeloma with rationally designed CAR T cells. Sci Transl Med. 2019;11(485):eaau7746.
56. Mikkilineni L, Kochenderfer JN. CAR T cell therapies for patients with multiple myeloma. Nat Rev Clin Oncol. 2021;18(2):71-84.